JOURNAL OF GEOPHYSICAL RESEARCH, VOL. 98, NO. B6, PAGES 9825–9844, JUNE 10, 1993

A Teleseismic Study of the Altiplano and the Eastern Cordillera in Northern Bolivia: New Constraints on a Lithospheric Model

CATHERINE DORBATH,[1,2] MICHEL GRANET,[2] GEORGES POUPINET,[3] AND CLAUDE MARTINEZ[1,4]

The Altiplano, one of the world's great plateaus, is the most significant geomorphological unit of the Central Andes. Knowledge of its lithospheric structure is essential to the understanding of the mountain building in this region. In order to study this, we performed a teleseismic field experiment in northern Bolivia. During a 4-month period, 34 short-period seismic stations were installed along a 320-km-long profile, crossing the Altiplano and the Eastern Cordillera, from the volcanic arc zone to the sub-Andean zone, perpendicular to the main structural direction. A careful study of relative travel time residuals led us to propose a qualitative model related to the structural patterns; the maximum amplitude of these residuals along the profile reaches 3 s for *P* phases and have a strong azimuthal dependence. The residuals show a noticeable sudden increase, clearly associated with the fault system bordering the Eastern Cordillera to the west, the Cordillera Real fault system. The high quality of the data allows us to perform a velocity inversion and to calculate at what depth lateral variations occur. The origin of the perturbations in the upper crust is reasonably accounted for by the depth variations of the sedimentary fill, with the maximum thickness found under the Altiplano basin. The velocity perturbations in the lower crust are interpreted as variations of the Moho depth which decreases from about 60 km below the Altiplano to 50 km below the Eastern Cordillera. In the upper mantle, a high-velocity zone is observed below the Eastern Cordillera. The major feature of this model is a subvertical boundary, dipping slightly to the southwest, which separates two strongly contrasting velocity units throughout the model, from the surface down to 140 km. This boundary coincides with the Cordillera Real fault system and is interpreted as an old suture. As the Altiplano is characterized by low velocities in the crust, the high velocities beneath the Eastern Cordillera down to 120 km may correspond to the Brazilian craton; in the region studied, the western limit of the underthrusting of the craton corresponds to the western border of the Eastern Cordillera.

INTRODUCTION

One of the prominent characteristics of the Andean chain is its segmentation along the strike [*Jordan et al.*, 1983]. This segmentation is directly related to the shape of the subducted Nazca plate. The part of the Andes, between 13°S and 27°S (in southern Peru, Bolivia and northern Chile), where the angle of dip of the subducting plate has a constant value of 30°, is called the Central Andes; it is characterized by specific tectonic features (Figure 1). This zone is divided, from the Pacific Ocean to the Brazilian craton, into nearly parallel morphological structures: a coastal range, an axial valley, the high volcanic arc called the Western Cordillera, the Altiplano (or Puna), the Eastern Cordillera, and the sub-Andean zone.

The most significant geomorphological unit of this segment is the Altiplano, a high plateau extending from southern Peru to northwestern Argentina, with a mean elevation of nearly 4000 m. In Bolivia, its width is about 450 km. It is, after Tibet, the largest high plateau in the world; however, its structure and development are by far less understood than those of the Tibetan Plateau.

Mountain building in the Central Andes is undoubtedly a very complex process. For a long time, it was assumed that the Altiplano was an extensional basin [*Aubouin et al.*, 1973]. However, recent tectonic and structural studies emphasize the compressive regime throughout the history of the chain [*Baby et al.*, 1990; *Martinez and Seguret*, 1990]. The main question is how such a large structure as the Altiplano was produced and maintained at such a high altitude. Several compensatory mechanisms have been proposed. The thickening of the crust can be due either to shortening or to magma addition. A number of hypothesis for the shortening mechanism have been proposed by authors in different ways. *Rutland* [1971] suggested crustal doubling by addition of subducted crustal material. *Uyeda and Kanamori* [1979] proposed thickening of the crust by folding for the Chilean type subduction. *James* [1971] combined folding and thrust faulting in his model. Underthrusting of continental crust is the mechanism proposed by *Bourgois and Janjou* [1981], *Suarez et al.* [1983], *Lyon-Caen et al.* [1985], *Isacks* [1988], and *Roeder* [1988]. Magma addition is suggested by *Dewey and Bird* [1970]. *Froidevaux and Isacks* [1984] have proposed that the topography is compensated by a combination of crustal thickening and lithospheric thinning. Finally, *Kono et al.* [1989] proposed a model with two coexisting processes between the two cordilleras to form the high plateaus (Altiplano and Puna): magmatism and crustal accretion are dominant at the western margin of the mountain system and their effects decrease eastward, while compression and the consequent crustal shortening are most important at the eastern margin and decrease toward the west.

A precise knowledge of the deep structure beneath the Altiplano is important for the understanding of the formation of the Andes. Seismic tomography has proved to be a powerful tool in studying velocity structures, especially in tectonically active regions [*Aki*, 1981]. In order to improve

[1]Institut Francais de Recherche Scientifique pour la Développement en Coopération, Paris.
[2]Ecole et Observatoire de Physique du Globe, Strasbourg, France.
[3]Laboratoire de Géophysique Interne et de Tectonophysique, Grenoble, France.
[4]Laboratoire de Géologie des Bassins, Montpellier, France.

Copyright 1993 by the American Geophysical Union.

Paper number 92JB02406.
0148-0227/93/92JB-02406$05.00

ORSTOM Fonds Documentaire
17 JUIL. 1995
N° : 41851 ex 1
Cote : B

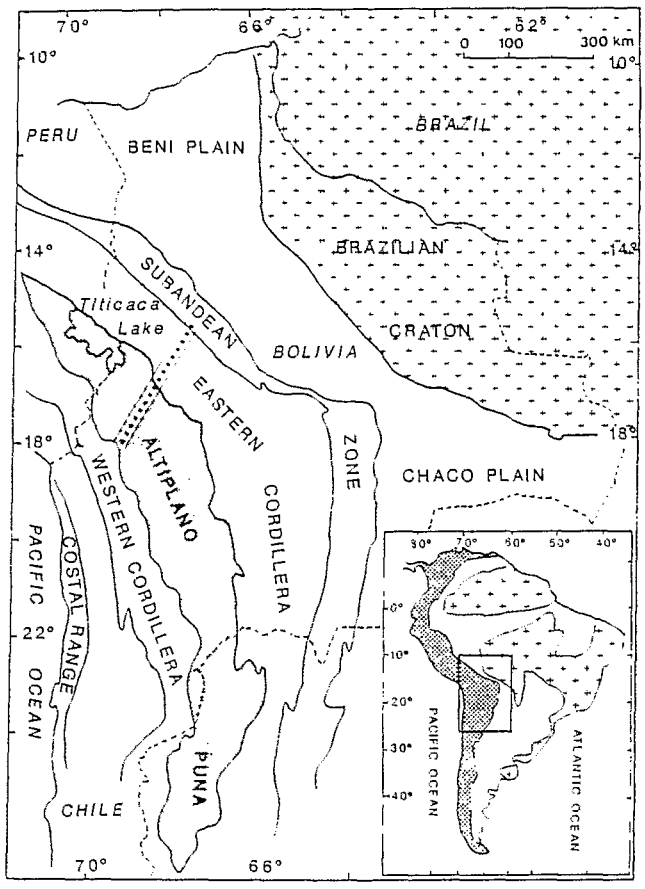

Fig. 1. Morphostructural zoning of the Central Andes. From the Pacific Ocean to the Brazilian craton (area marked with crosses), the main units are the coastal range, the axial valley, the Western Cordillera, the Altiplano-Puna region (shaded area), the Eastern Cordillera, and the sub-Andean zone. Crossing the Altiplano and the Eastern Cordillera, between 15° and 18°S and 67° and 69°W, the dotted line represents the approximate location of the teleseismic study described in this paper. The rectangle in the inset shows the location of the Central Andes in South America.

our knowledge of the deep structure beneath the Central Andes, we have performed a teleseismic field experiment in northern Bolivia, from the border of Chile to the Rio Beni passing through La Paz (Figure 2). The seismic profile crosses two main morphological units of the Andean chain: the Altiplano and the Eastern Cordillera. It starts in the volcanic arc and extends 25 km into the sub-Andean zone, approximately perpendicular to the main structural trend of N320°W.

The aim of this paper is to use *P* teleseismic delay times to perform a tomographic inversion of the lithosphere and to map the relative velocity perturbations beneath the Altiplano and the Eastern Cordillera. In particular, we will determine how and where the deep transition between these two structural units occurs. The spacing between the stations, together with the teleseismic wavelength, will also allow us to obtain information about the sedimentary fill. Results from this study, in addition to previous geophysical works and crustal seismic studies undertaken concurrently (G. Herquel et al., Crustal structure of the Altiplano and the Eastern Cordillera in northern Bolivia from regional earthquake analysis and amplitude coherency at teleseismic distances, submitted to *Geophysical Research Letters*, 1992), will provide new constraints on a lithospheric model and therefore on mountain building in the Central Andes.

Structural Setting

This study was situated at the latitude of Bolivia and northern Chile where the Andean Cordillera changes its trend from the northwest-southeast direction in the north, to an overall north-south direction in the south (Figure 1). The seismic profile was located across the northwest-southeast segment of the Bolivian Orocline.

Important compressional crustal shortening in the modern Andes is currently accepted [*Audebaud et al.*, 1973; *Martinez and Tomasi*, 1978; *Sheffels*, 1988, 1990; *Roeder*, 1988; *Sempere et al.*, 1990]. However, the interpretation of the crustal cross section in the sector studied differs from one author to another. In the most recent works the Andean deformation is interpreted as a low-angle transcrustal thrusting (Main Andean Thrust (MAT) of *Roeder* [1988]; Cabalgamiento Andino Principal (CANP) of *Sempere et al.* [1990]), which overlaps northeastward the Andean foreland for more than 200 km. Above the MAT and southwest and northeast of the Eastern Cordillera, there are low-angle dipping thrusts which are respectively southwest and northeast vergent. These thin-skinned-type interpretations do not account for all the observed geological data. For example, in spite of its sedimentary fill of 15 to 20 km thickness [*Meyer and Murillo*, 1961; *Ascarrunz*, 1973*a*, *b*], the wide northern Altiplano Basin does not appear on such sections, nor do the major high-angle faults appear which are frequently observed in the field, such as the San Andres fault, the Coniri fault, the Cordillera Real fault [*Ascarrunz*, 1973*a*; *Martinez*, 1980; *Lavenu*, 1986; *Martinez and Seguret*, 1990]. The important deformation associated with magmatic activity and metamorphism developed during Early to Late Paleozoic ("Hercynian phases") is ruled out by *Roeder* [1988], whereas it has been readily demonstrated to exist in the Eastern Cordillera of Peru and Bolivia by *Megard et al.* [1971], *Bard et al.* [1974], *Martinez et al.* [1972], *Dalmayrac et al.* [1980], and *Martinez* [1980].

The structural zones of the Andean belt roughly correspond to the morphological units (Figures 1 and 2*b*): to the east of the main volcanic arc, the intracordilleran Tertiary Altiplano Basin is juxtaposed to a belt of folded Paleozoic sedimentary rocks, evidence of a Hercynian belt centered on the Eastern Cordillera of Bolivia and southern Peru [*Martinez and Tomasi*, 1978; *Martinez*, 1980; *Dalmayrac et al.*, 1980]. On the northeastern flank of the Eastern Cordillera, a zone of large longitudinal faults (MAT, see above) marks the transition into the sub-Andean zone, in which strike belts involve Neogene rocks and are clearly Andean in age. These main morphostructural zones, which are individually affected by major faults, can be differentiated into different units (Figures 2*a* and 2*b*).

Altiplano Domain

In its northern part, the Bolivian Altiplano (4000 m high) is dissected by a longitudinal and transverse network of faults: the longitudinal "San Andres fault zone," separates the volcanic western Altiplano from a central Altiplano Basin which subsided during Cenozoic time.

In the western Altiplano (stations 1–5, Figure 2*a*), the

Quaternary volcanic cones are up to 6000 m high. In this area, the Quaternary lava and the Miocene and Plio-Pleistocene volcanic-detrital and ignimbrite materials overlay a Mesozoic series known only on the base of the San Andres borehole [*Lehmann*, 1978]. According to drill data, the Paleozoic rocks are not present, and the Precambrian basement (at 2745 m depth) includes gneisses and granites. The San Andres fault zone is interpreted to be the eastern border of the Precambrian Arequipa terrane [*Martinez*, 1980] which is the remains of the Late Precambrian–Early Cambrian Brasilides [*Lehmann*, 1978], consisting of reworked rocks dated 1100–1900 Ma and 2000 Ma [*Cobbing et al.*, 1977].

The Altiplano Basin (stations 7–13, Figure 2*a*) extends east of the San Andres fault system. This subsiding Cenozoic intracordilleran basin is divided by transverse and longitudinal faults which delimit blocks of varying sizes and subsidence rates. Along the zone of the profile, across a 200-km-long syncline, with a north-northwest/south-southeast axis, the Cenozoic detrital series, which is as recent as Pliocene, is more than 10 km thick. The total thickness of sedimentary rocks including the underlying Paleozoic, Mesozoic and Paleogene beds, is about 20 km [*Meyer and Murillo*, 1961; *Ascarrunz*, 1973*a*, *b*]. The western limit of the basin is marked by the "Coniri fault zone" which is transformed to the southeast of Patacamaya by the sinistral strike-slip "Laurani fault zone", through a zone of hidden transfer faults ("Ayo Ayo fault zone" [*Ascarrunz*, 1973*b*]).

In the Altiplano Basin, to the north of the profile, *Martinez and Seguret* [1990] have confirmed the occurrence of considerable subsidence and have shown that sedimentation is contemporary with the compressive deformation which was continuous from the Eocene to the Pliocene. During Cenozoic, thrusting of opposite vergence along the San Andres fault zone and the Corocoro thrust [*Martinez*, 1980] resulted in folding and thrusting of the subsiding basin compressed between the Precambrian of the Arequipa terrane and the Paleozoic rocks of the Eastern Cordillera. This synsedimentary deformation is particularly marked toward the edges of the basin in contrast with the apparent simplicity of the medial syncline.

East of the Coniri-Laurani fault zone, Paleozoic rocks crop out through a reduced Cenozoic cover in the ridges that separate basins. Although located in the morphological Altiplano, these Paleozoic ridges belong to the western limb of the geological Eastern Cordillera [*Sempere et al.*, 1990].

Eastern Cordillera Domain

The Eastern Cordillera is divided into three zones, from west to east: the western flank, the Cordillera Real fault zone (CRFZ) and the axial zone. The Paleozoic rocks which underlie the Eastern Cordillera have been deformed during the Early and Late Paleozoic ("Hercynian") before being further deformed by Andean compressions.

The western flank of the Cordillera ("Huarina fold-thrust belt" [*Sempere et al.*, 1990]) extends from the Coniri–Laurani faults to the Cordillera Real fault system (stations 15–20, Figure 2*a*). The Paleozoic series (mostly Silurian to Devonian) is 10–12 km thick. Hercynian folds have been deformed during Andean tectonics by southwest thrusting and locally by northeastern vergent backthrusts. Silurian-Devonian series are frequently thrust over the syncline developed after the Cretaceous, during Oligo-Miocene and Pliocene times.

The Cordillera Real fault zone (stations 21–23, Figure 2*a*) corresponds to a steeply dipping northwest-southeast trending faults, set in left-lateral en échelon system and which suffered multiple extensional and compressional reactivation [*Martinez*, 1980; *Lavenu*, 1986]. It is bounded to the east by the Oligo-Miocene granodioritic batholith (Cordillera Real, Illimani, Quimsa Cruz) [*McBride et al.*, 1983]. Its trace is roughly parallel to the Cordillera Real thrust of *Sempere et al.* [1990].

In the axial zone (stations 24–31, Figure 2*a*), the detrital Ordovician series which forms the main part of the outcrops is up to 5000 m thick. The Ordovician series was folded and metamorphosed during Hercynian phases and has been intruded, close to the CRFZ by (1) syntectonic Zongo-Yani monzogranites [*Bard et al.*, 1974], (2) Triassic plutons [*McBride et al.*, 1983], and (3) Oligo-Miocene granites. In the axial zone, the Andean tectogenesis is superposed on the Hercynian magmatism and deformation. The Andean reverse faults and thrusts have a northeast vergence.

The axial zone is bounded on the northeastern flank by a narrow belt of Silurian-Devonian rocks and by the Main Andean thrust system which separates the Eastern Cordillera from the sub-Andean zone whose Paleozoic and Meso-Cenozoic series is probably over 10 km thick (stations 32–34, Figure 2*a*).

Therefore the CRFZ appears to form the most prominent tectonic boundary of the section studied, loci of repeated magmatic activity, and a boundary between northeast and southwest vergent Andean thrusting. We can also note that it corresponds to an anomaly of electric discontinuity detected by *Schmucker et al.* [1966].

PREVIOUS GEOPHYSICAL RESULTS

In order to image the deep lithosphere, we have to select an initial velocity model. This requires a reasonable knowledge of the crustal structure, namely, the vertical velocity distribution and the Moho depth. These data are provided mainly by seismic refraction and reflection experiments. Since the wavelength of the teleseismic waves we used for the inversion (about 10 km) is not sensitive to small-scale perturbations, in this first part we will concentrate on the thickness of the crust and will not discuss the detailed velocity distribution.

The first deep seismic sounding was carried out during the International Geophysical Year, 1957, by the Carnegie Group [*Tatel and Tuve*, 1958]. New seismic profiles along the Altiplano were performed in 1968 [*Ocola et al.*, 1971, *Ocola and Meyer*, 1972]. Using secondary arrivals, the latter postulated a crustal thickness greater than 70 km. More recently, seismic profiles have been performed in northern Chile and southern Bolivia [*Wigger*, 1988], but as a result of the high attenuation beneath the Altiplano, the structure is not well constrained. According to *Wigger* [1988] the depth of the Moho beneath the Altiplano should not exceed 76 km. While this value is based on some weak indication of *S* wave arrivals, there is no evidence for this discontinuity with *P* waves. Last, a crustal refraction study undertaken, concurrently with this work, using regional earthquakes as sources, shows a crustal thickness of 60 to 70 km (G. Herquel et al., submitted manuscript, 1992).

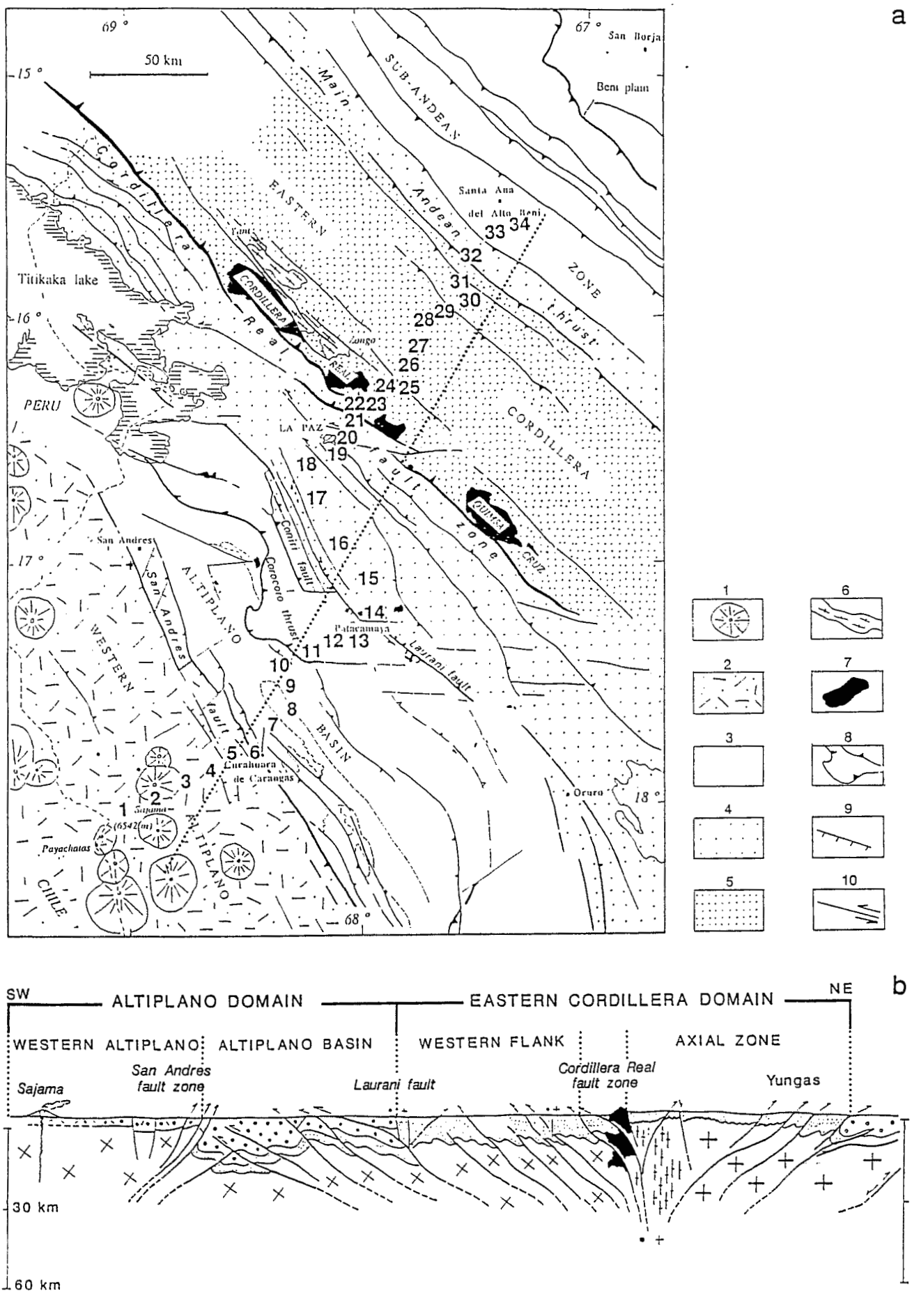
a
69 °
67 °
15 °
16 °
17 °
18 °
68 °
50 km
San Borja
Beni plain
Main
SUB-ANDEAN
ZONE
Andean
thrust
Santa Ana
del Alto Beni
EASTERN
CORDILLERA
Real
Cordillera Real
Titikaka lake
PERU
CHILE
LA PAZ
Sajama
(6542 m)
Payachatas
San Andres
San Andres fault
WESTERN
ALTIPLANO
Coniri fault
Corocoro thrust
Patacamaya
Laurani fault
Curahuara
de Carangas
Oruro
BASIN
Quimsa Cruz
fault
zone
1
2
3
4
5
6
7
8
9
10
b
SW
NE
ALTIPLANO DOMAIN
EASTERN CORDILLERA DOMAIN
WESTERN ALTIPLANO
ALTIPLANO BASIN
WESTERN FLANK
AXIAL ZONE
Sajama
San Andres
fault zone
Laurani fault
Cordillera Real
fault zone
Yungas
30 km
60 km

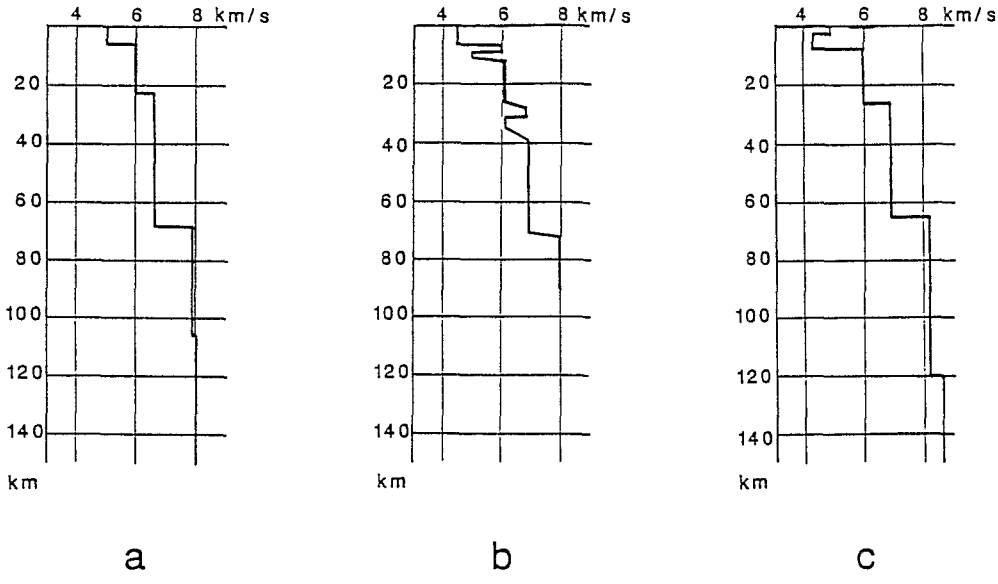

Fig. 3. Previous P velocity models for the region under study: (*a*) *James* [1971] from surface waves analysis, (*b*) *Ocola et al.* [1971] for the Altiplano from seismic refraction, (*c*) Molina for La Paz [from *Cabré*, 1983], from P and S residuals study.

After the pioneering work of *Cisternas* [1961], phase and group velocities of Rayleigh and Love waves have been used by *James* [1971] to derive models of the crust and upper mantle beneath the Central Andes. The crustal thickness inferred from this study is about 70 km beneath the Western Cordillera and the western part of the Altiplano, thinning to 50–55 km beneath the Eastern Cordillera. However, the reliability of these results is limited because the interpretation of the data assumes horizontal layering in a region where the topography of the interfaces is strongly disturbed.

Also some local studies have been performed in Bolivia: the Moho depth beneath La Paz was found to be 65 km by the spectrum of longitudinal seismic waves [*Fernandez and Careaga*, 1968] as well as by the inversion of both P and S wave residuals [*Cabré*, 1983]. Figure 3 presents three of the velocity models described above.

Some crustal models have been calculated from gravity anomalies. In northern Chile and southern Bolivia (20°–24°S), the interpretation of new gravity measurements provides a moho depth of 60 km under the Western Cordillera, decreasing to the east [*Strunk*, 1990]. Finally, modeling of new gravity data, crossing the Central Andes in Peru (14°S), through the northern part of the Altiplano, gives a Moho depth of 65 km under the Western Cordillera and 55 km under the Eastern Cordillera [*Fukao et al.*, 1989]. The increase of nearly 150 mGal, occurring where the Eastern Cordillera is bordered by the flat lands of the Amazon Basin, suggests a sudden change in the crustal thickness of about 15 km.

In conclusion, from these seismic and gravity measurements, no definitive crustal model has been established for the region to the present day. However, most authors agree on a crustal thickness beneath the Altiplano of the order of 60–70 km, decreasing to 50–55 km beneath the Eastern Cordillera. This uncertainty in crustal thickness should have an only minor influence on the results of the inversion procedure, especially concerning the subcrustal lithosphere structure, as long as there is no strong vertical coupling observed during the inversion process.

FIELD EXPERIMENT AND DATA PROCESSING

Between October 1990 and February 1991, 34 temporary digital recorders of the French Lithoscope network, equipped with vertical short-period seismometers (Mark Product L4C, $T_0 = 1$ s) were installed along a profile crossing the Altiplano and the Eastern Cordillera. This profile (Figure 2*a* and Table 1) is roughly perpendicular to the direction of the main Andean structures, which show an axial symmetry. Station locations were strongly dependent on the availability of usable roads. This problem was crucial on the eastern flank of the Eastern Cordillera, from station 24 to station 29, where the road descends from the Cordillera, 3200 m high, to the "Yungas", 900 m high, in a very narrow valley. There it was impossible to find sites with low seismic noise level, which were far from the disturbance of the traffic. This difficulty is the main cause of the lack of data at some of these stations.

The total length of the profile is 320 km, with a mean station spacing of 10 km, adapted to the wavelength of teleseismic P waves. Time was provided by internal clocks controlled by a master clock.

During a period of $3\frac{1}{2}$ months, while all the stations were running simultaneously, we recorded nearly 500 seismic

Fig. 2 (Opposite). (*a*) Geological setting of the region under study. The numbers of the legend refer to the different geological and tectonical units: 1, Quaternary volcanoes; 2, Cenozoic volcano-sedimentary cover; 3, Meso-Cenozoic Altiplano Basin and Paleozoic-Mesozoic-Cenozoic sub-Andes; 4, Siluro-Devonian borders of the Eastern Cordillera; 5, Ordovician axial zone of the Eastern Cordillera; 6, Hercynian plutons; 7, Andean plutons; 8, thrust fault; 9, normal fault; and 10, strike-slip fault. The bold numbers show the location of the temporary seismic stations. The dotted line displays the location of the cross sections presented in Figure 2*b* and Plate 3. (*b*) Geological and structural cross section; the same symbols as on Figure 2*a* are used.

TABLE 1. Stations Coordinates

	Name	Code	Latitude, °S	Longitude, °W	Altitude, m
1	Mujtalla	MUJT	18.0581	68.9656	4338
2	Caripe	CARI	18.0032	68.8408	4230
3	Tolatia	TOLA	17.9388	68.7384	4077
4	Catacora	CATA	17.9135	68.6169	3920
5	Kelkata	KELK	17.8436	68.5331	3900
6	Curahuara	CURA	17.8261	68.4269	3912
7	Bella Vista	BEVI	17.7208	68.3715	3901
8	Posotalla	POSO	17.6435	68.2963	3880
9	Corapi	CORA	17.5393	68.3060	3806
10	Huarejani	HUAR	17.4382	68.3152	3896
11	Pokullita	POKU	17.3840	68.2294	3994
12	Huancarames	HUAN	17.3601	68.1123	3901
13	Copani	COPA	17.3286	68.0553	3872
14	Patacamaya	PATA	17.2604	67.9480	3804
15	Pumasani	PUMA	17.0774	67.9735	3955
16	Pinalla	PINA	16.9432	68.1110	3980
17	Pocohota	POCO	16.7519	68.1923	3980
18	Ventilla	VENT	16.6223	68.1747	3960
19	LaPaz	LAPZ	16.5363	68.1000	3300
20	Vinto Pampa	VIPA	16.4679	68.0798	3500
21	Incachaca	INCA	16.4085	68.0480	4366
22	Rinconada	RINC	16.3237	68.0196	4210
23	Unduavi	UNDU	16.3312	67.9495	3590
24	CotaPata	COTA	16.2849	67.8496	3219
25	Chuspi Pata	CHUS	16.3050	67.8152	3000
26	Yungas	YUNG	16.2344	67.7935	2000
27	Puente Mururata	PUEN	16.1658	67.7285	1100
28	Hotel du Planteur	HOTE	16.0421	67.6643	1100
29	San Pedro de Leon	SPDL	16.0047	67.6193	930
30	San Silverio	SILV	15.9236	67.5415	970
31	Colonia Saonedra	CBSA	15.8494	67.5275	634
32	Colonia Bartos	BART	15.7428	67.5028	927
33	Thee	THEE	15.6462	67.4262	1003
34	Rio Beni	BENI	15.5674	67.3711	489

events; of those, only 200 were reported by international bulletins, 85 of which were teleseismic events. Only 57 events which show a clear *P* wave onset were finally used in this study. Their epicentral distance and azimuth distribution is plotted on Figure 4. *P* and *PKP* phase arrival times were measured using waveform matching across the network. Special attention was paid to core phases for events with epicentral distances between 136° and 146° to avoid possible incorrect identification among the different phases. The overall accuracy of the relative arrival times is estimated to be better than 0.1 s. The final data set contains 595 observations.

Absolute travel times were calculated using National Earthquake Information Center (NEIC) hypocenter parameters and *Jeffreys and Bullen* [1970] travel time tables for *P* phases. We preferred to use *Herrin*'s [1969] tables for *PKP* phases because his travel time curve is more detailed and precise for the core phases. These allowed us to use phases from the three *PKP* branches according to the epicentral distance. This choice of two travel time tables will not produce artifacts in the timing procedure because we only used relative residuals. Travel times were corrected for station elevation, assuming the same crustal velocity as in the first layer of the starting model used for the inversion (Table 2). It was not possible to correct travel times for variations in the sedimentary cover because of the lack of precise information concerning velocities and thicknesses of the various formations.

The absolute travel time residuals contain large contributions from hypocenter and origin time errors, and from the differences between the average earth model and the actual path from source to receiver. Given the distance from source to receiver, for teleseismic events, these errors are nearly constant across reasonably small arrays. They are removed effectively by forming relative residuals, computed by subtracting a reference residual (representative of the receiver array for a particular event) from each absolute residual. For the reference residual, one may use the residual at some reference receiver believed to be outside the most anomalous region, or an average residual [*Evans and Achauer*, 1993]. In the case of the Bolivian experiment, some stations, particularly on the eastern flank of the Eastern Cordillera, did not record every event. The lack of data corresponding to these stations for some events could introduce a bias when calculating the mean residual for these events. Thus we took station 10 as a reference. This station is situated in the central part of the Altiplano, far from any major structural change. It was operational throughout the whole of the experiment and recorded all the events. The position and the continuous operation of this station make it a convenient reference.

Another problem specific to this experiment is caused by the presence of velocity anomalies associated with subduction. A precise location of local events recorded during this field experiment shows that the subducted slab is 160 km below the western end of the seismic profile, extending down to 220 km in the middle part of the profile (C. Dorbath and M. Granet, Local earthquake tomography of the Altiplano

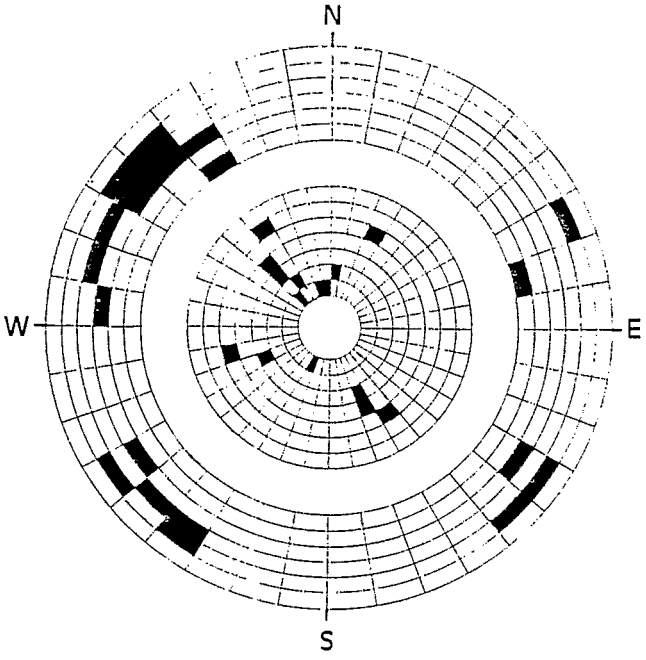

Fig. 4. Distance and azimuth distribution of the teleseismic events used in this study with an increment of 10°. They are plotted relative to La Paz, approximately the center of the seismic array. Each shaded sector corresponds to an average of two events: inner circles, for *P* phases (between 20° and 90°), and outer circles, for *PKP* phases (between 120° and 180°).

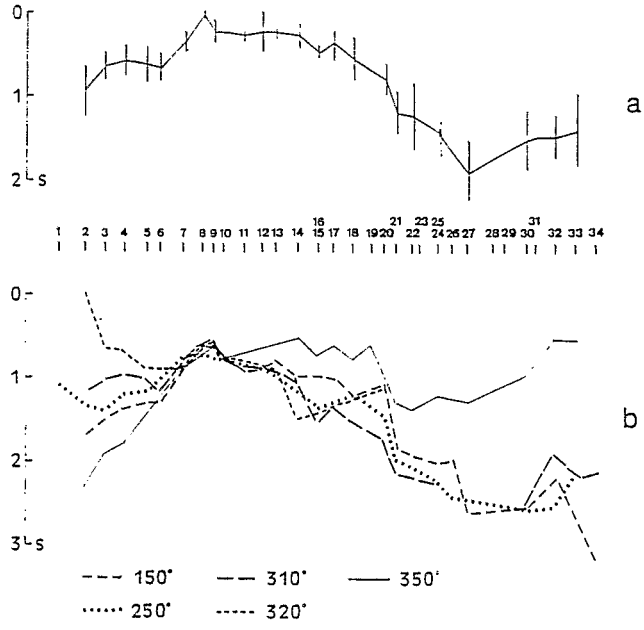

Fig. 5. Relative residuals representations: (*a*) mean *PKP* residuals relative to station 10 (HUAR). They are averaged on the whole azimuthal range and plotted along the profile with the corresponding standard errors. (*b*) *P* residuals, relative to station 10, according to five different azimuths for which a number of events was recorded.

and the Eastern Cordillera of northern Bolivia, submitted to *Journal of Geophysical Research*, 1993). Thus it will not be possible to map the slab in this work. However, depending on the epicentral distribution, the teleseismic rays may or may not cross the slab. This would only be the case for the Columbian and Venezuelian earthquakes, with ray paths from the north and at short epicentral distance (20°–30°). These slab-perturbed travel times do not influence our model.

VARIATION OF RELATIVE RESIDUALS

The data set is nearly equally divided into *P* and *PKP* phases. Due to the quasi-vertical incidence of *PKP* phases, no azimuthal variation of the corresponding residuals is observed. A plot of the mean *PKP* relative residuals (Figure 5*a*) gives a crude picture of the lateral velocity variations. However, the azimuthal- and distance-dependent variation of *P* residuals is the main basis for imaging spatial and depth velocity perturbations from a spherically symmetric Earth velocity model. Figure 5*b* shows representative examples of these mean relative *P* residuals along the profile for events occurring at different azimuth ranges.

The southeastern stations (1–6) show a pronounced azimuthal variation. The residuals increase rapidly as the azimuths of the epicenters turn counterclockwise from N350°W to N320°W. The amplitude of the variation is very large, 2.4 s at station 2, and progressively vanishing to the east. The behavior of the azimuthal variations is indicative of a strong lateral velocity change with a strike of about N330°W passing close to station 6.

From station 7 to station 13, the amplitude of the azimuthal variations is small. From station 14 to station 20, the relative residuals are more dispersed, and no simple azimuthal effect can be seen. The amplitude of the variation is of the order of 0.8 s.

For all azimuths a major change in the shape of the profiles is observed between stations 19 and 21. It consists of a sharp and significant decrease of the relative residuals by about 0.5 s.

From station 21 to station 34, two distinct groups are observed on the profiles. The difference between the relative residuals of these two groups is 1.5 s from station 27 to station 34. While the events coming from the N350°W azimuth present the highest residuals, those coming from the N310°W azimuth are in the lower group. This behavior indicates a lateral velocity change with a strike of approximately N320°W passing close to station 20.

Another way to study the azimuthal and spatial variations of teleseismic *P* residuals is to express them in polar diagrams [*Dziewonski and Anderson*, 1983]. Following *Babuska et al.* [1984], relative residuals obtained by averaging the absolute residuals for selected events are plotted in a stereographic projection giving the diagrams shown in Plate 1. We grouped all events into regions using sliding windows of 15° for azimuth and 4° for angle of incidence to decrease the effects of an uneven distribution of earthquakes. A cubic spline function was used to interpolate and smooth the data (courtesy of Y. Liotier). The residuals shown in Plate 1 are corrected for the elevation and, in this particular case,

TABLE 2. Initial P-Velocity Model

Layer	Thickness, km	Velocity, km/s
1	30	6.2
2	30	6.8
3	40	8.0
4	40	8.1

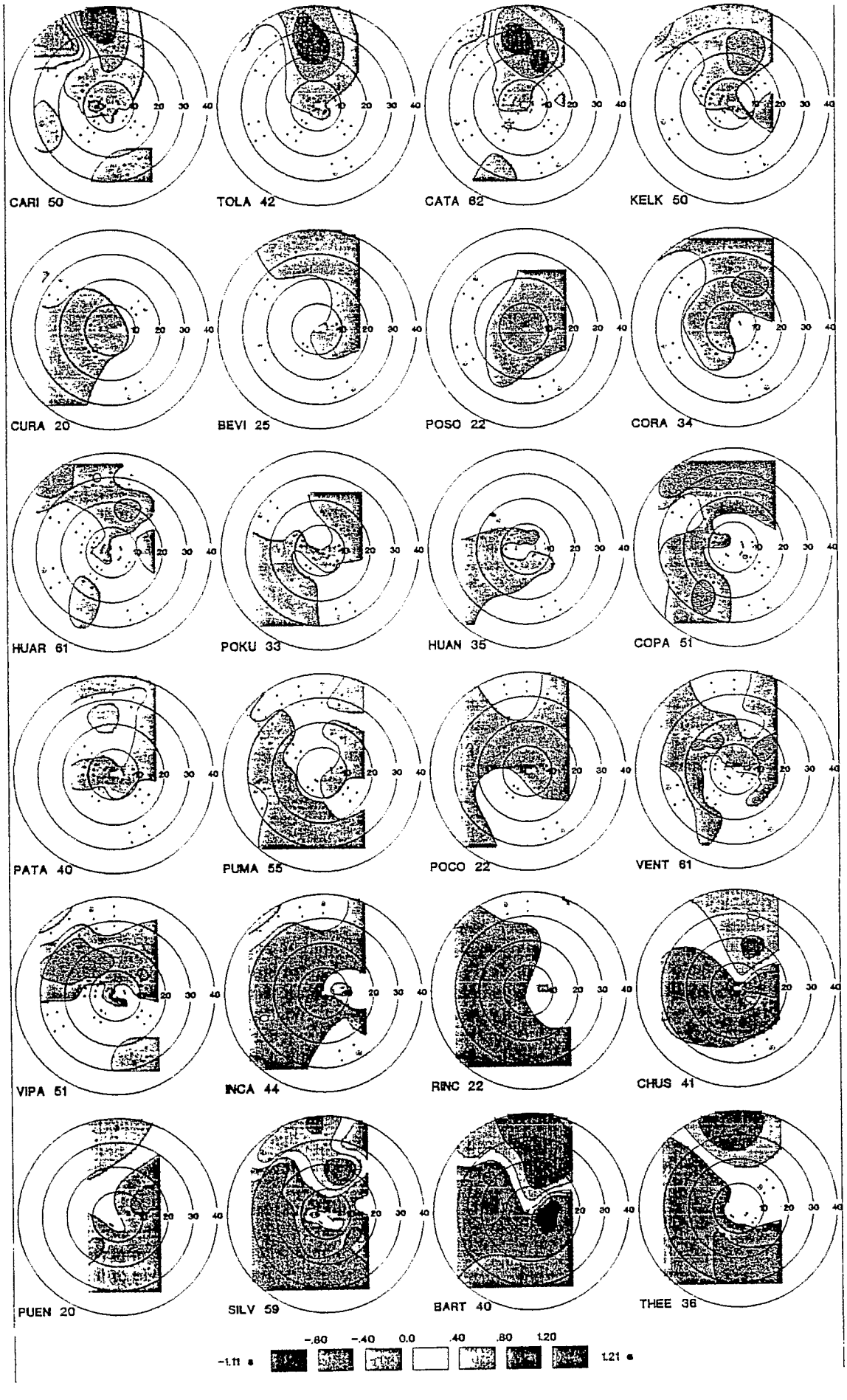
CARI 50
TOLA 42
CATA 82
KELK 50
CURA 20
BEVI 25
POSO 22
CORA 34
HUAR 61
POKU 33
HUAN 35
COPA 51
PATA 40
PUMA 55
POCO 22
VENT 61
VIPA 51
INCA 44
RINC 22
CHUS 41
PUEN 20
SILV 59
BART 40
THEE 36
-.80
-.40
0.0
.40
.80
1.20
-1.11 s
1.21 s

normalized to an average residual as described above. This normalization is valid because we constructed the polar diagrams using only the events for which there is at least one station in each geological zone defined on Figure 2. This procedure will allow us to study the behavior of our reference station (HUAR, station 10). For each diagram, the zero level represents the relative residual averaged over all of the source regions.

Lithospheric structures have a dominating influence on the diagram pattern. The latter is influenced mainly by oriented structures beneath a station and inhomogeneities in the mantle. All seismological stations exhibit a strong dependence of *P* residuals on azimuths and incidence angles.

For stations 2–5 (CARI, TOLA, CATA, KELK) all waves travelling from the north are relatively fast compared to their representative average and the largest negative values of the residuals are observed for these stations. Station 6 (CURA) shows a different pattern (the fast direction is southwest) with small amplitudes of the residuals (±0.4 s).

From station 7 to 13 (BEVI, POSO, CORA, HUAR, POKU, HUAN, COPA), the azimuthal dependence of the *P* residuals is less marked than for stations 2–5. These stations can be separated into two groups. The first group, consisting of stations 7 (BEVI), 8 (POSO), and 9 (CORA), is characterized by fast waves travelling from the north and northeast, while the other group, stations 11 (POKU), 12 (HUAN), and 13 (COPA), shows more pronounced fast arrivals from the south and southeast. Station 10 (HUAR), which has recorded the full set of teleseismic events, shows an intermediate and relatively simple pattern. This supports our choice of station 10 as the reference station.

From station 14 (PATA) to station 18 (VENT), the polar diagrams show almost the same coherent and simple pattern with waves coming from the north and the south being slow. Station 20 (VIPA) when compared to the latter ones exhibits a similar pattern; waves arriving from the south are slow for all the epicentral distances, while for station 21 (INCA) and 22 (RINC) we observe a quite different polar diagram pattern. This is consistent with the *P* profiles (Figure 5*b*) where a significant decrease of the residuals is seen between stations 19 and 21. From station 25 (CHUS) to station 33 (THEE), the pattern of the polar diagrams changes gradually. A remarkable consistency in the behavior of the residuals for the stations in the sub-Andean zone (stations BART and THEE) is observed. The waves arriving from southern and southeastern azimuths are fast.

In summary, it is worth noting the consistency of these two residual studies with the structural units described above. A simple qualitative model with an axial symmetry can explain much of the gross variation of the relative residuals. This model, between stations 7 and 19, consists of a zone of slow material extending from the San Andres fault system to the Cordillera Real fault system. The strike of the lateral velocity changes, about N320°W, is in agreement with the Andean structural direction. The slowest part is observed beneath stations 7 and 14 and clearly corresponds to the central Altiplano Basin. A zone of high velocity is observed to the east of the Cordillera Real fault system. Figures 5*a* and 5*b* show a generally rapid velocity decrease between stations 14 and 27; in any case, this velocity contrast between the Altiplano Basin (station 14) and the central Eastern Cordillera (station 27) has to be very large in amplitude and/or extend to great depths to explain the observed variations (for example, a difference of 1.8 s is observed between these two stations in the case of vertical *PKP* rays). The careful study of the relative residuals leads us to a qualitative model; however, it does not allow us to determine at what depth the lateral perturbations occur. The data inversion will refine and quantify this simple model.

Plate 1 (opposite). Polar diagrams of a set of stations. The stations are referenced by their code name (see Table 1) and the number of data used for this specific study. Each diagram shows the average residuals for the source regions plotted as a function of the azimuth and incidence angle of the arriving waves. The outer perimeters of the diagrams correspond to the incidence angle of 40°, i.e., to waves from epicentral distances of about 20°. Fast directions correspond to negative values (blue end of the spectrum) and slow directions by positive values (red end of the spectrum).

DATA INVERSION

The starting *P* velocity model that was used for the teleseismic inversion (Table 2) is a smoothed version of the velocity models presented in Figure 3. The choice of a crustal thickness was not simple, as the Moho depth changes from 55 to 75 km depending on different authors; thus we have performed a number of computations with a Moho depth increasing from 50 to 80 km with a 5-km increment. Finally, we selected a Moho depth of 60 km below sea level as the best starting model for the inversion. The aperture of the profile allows us to image the lithosphere-asthenosphere system down to 140 km, and the short distance between the stations (about 10 km) results in a good lateral resolution without spatial aliasing.

The technique used here to invert the relative residuals [*Glahn et al.*, 1993] follows the method developed by *Aki et al.* [1977] and involves the partition of the volume under investigation into layers, which are themselves divided into blocks. As the network was quasi linear and perpendicular to the structures which exhibit an axial symmetry (Figure 2), we began with a two-dimensional inversion. The initial velocity model was divided into four horizontal layers: the crust, consisting of two layers each 30 km thick, is underlained by two layers each 40 km thick. Each layer was divided into 20 blocks of 20 km length. For the inversion, we kept only those blocks which were sampled by more than 10 rays. The model obtained reduces the data variance by 70%. As the initial variance is 0.29 s^2, the reading errors estimated as being 0.1 s can explain 20% of the data variance. The reduction of the variance obtained for the two-dimensional inversion is then satisfactory and demonstrates that the hypothesis of axial symmetry of the structures is a good approximation.

To further enhance our picture of the velocity perturbations and to cross-check our assumption of axial symmetry, we then performed a three-dimensional inversion. The initial velocity model selected was divided into layers of the same thickness as in the previous analysis and square blocks of the length of a third of a degree in each horizontal direction, with 12 blocks in the north-south direction and 10 in the east-west direction. We only retained the blocks sampled by more than 10 rays, as in the two-dimensional case. Since the geometry of the blocks is important in the method used to perform the inversions, we tested several different models. Our final block model, which takes into account the geometry of the

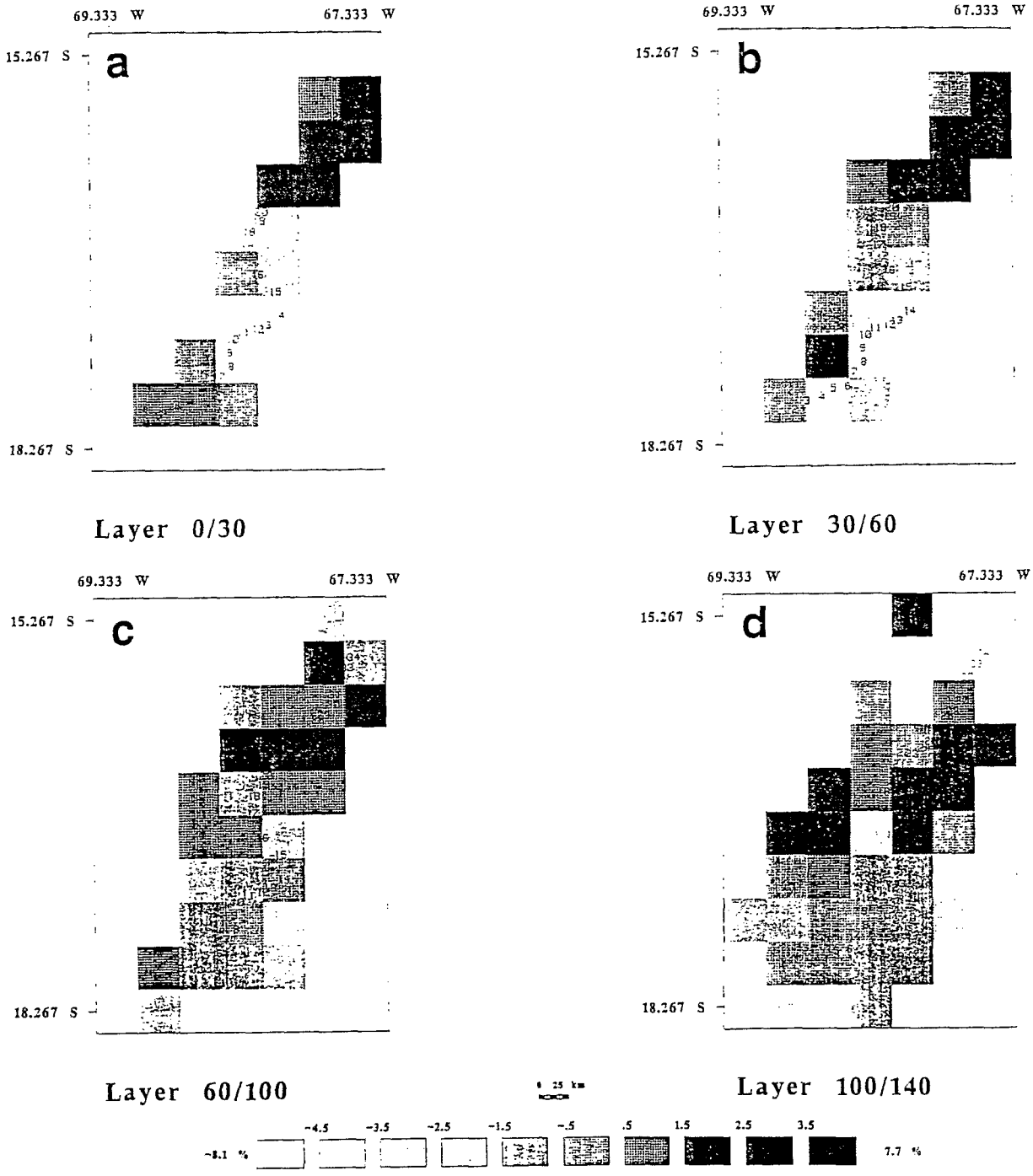

Fig. 6. Four-layer block model obtained by three-dimensional inversion of teleseismic P residuals. The velocity perturbations are given in percent with respect to the initial model (Table 2): a positive change indicates higher velocity and a negative change lower velocity.

network, has been chosen to avoid merging stations located on different structural units in the same block. The three-dimensional velocity model obtained by inversion is presented by blocks in Figure 6 as velocity perturbations in percent with respect to the reference model. The reduction of the variance obtained is just a little higher than with the two-dimensional model (72%).

Several tests have been performed to check the reliability

Fig. 7 (opposite). Results of the three-dimensional inversion for the synthetic residuals for studying the spatial resolution of the ray geometry as given in Figure 4. The starting velocity model, consisting of blocks with alternating +4% and −4% velocity perturbations in horizontal and vertical directions, is shown at the bottom of the figure. The recovery of the input model as velocity perturbations (in percent) obtained by the inversion of the synthetic residuals is shown for the four layers. White areas are not resolved due to less than 10 rays per block.

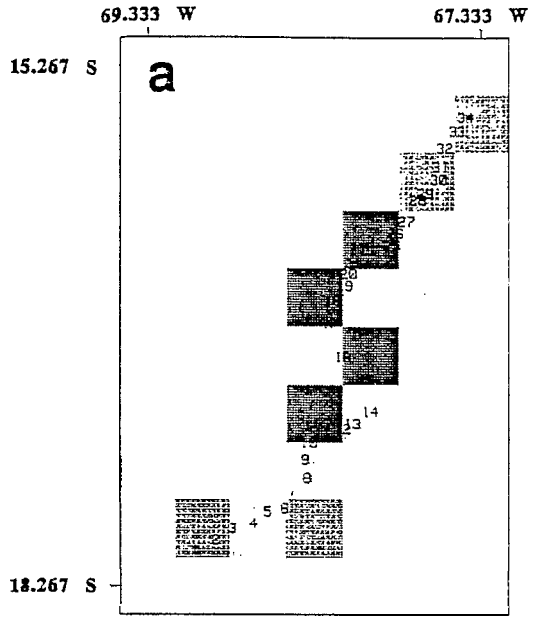

Layer 1: 0-30

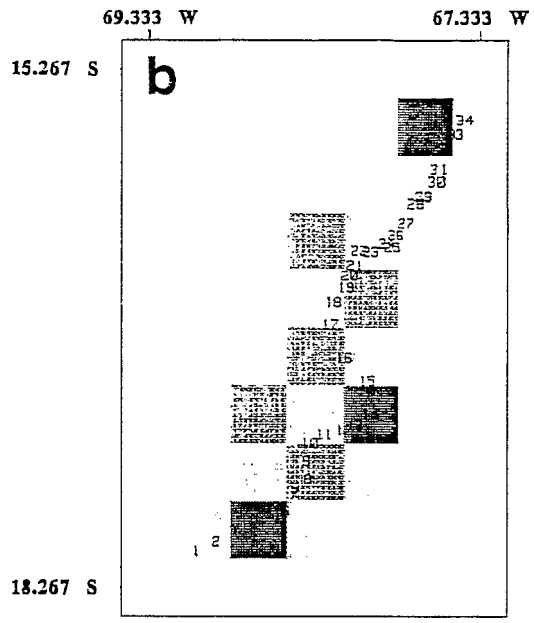

Layer 2: 30-60

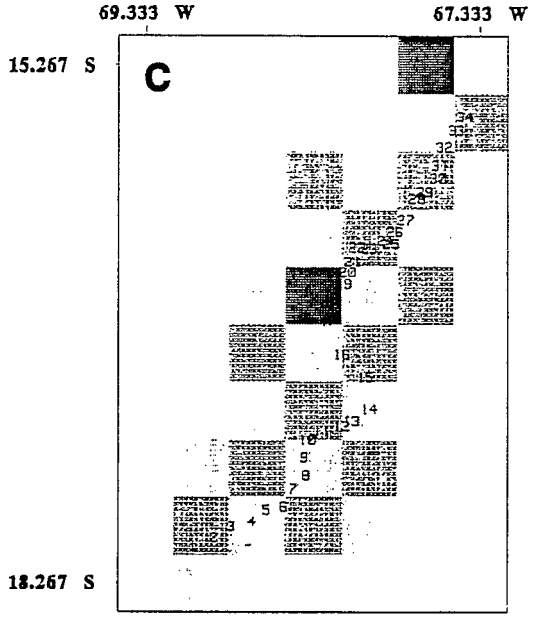

Layer 3: 60-100

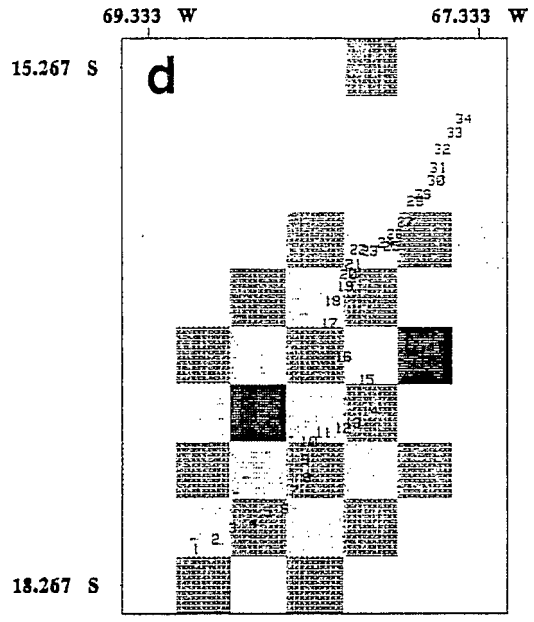

Layer 4: 100-140

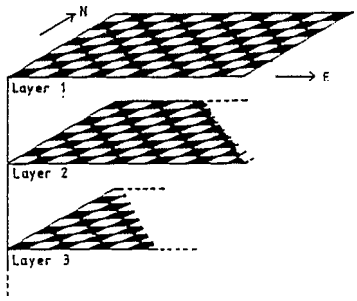

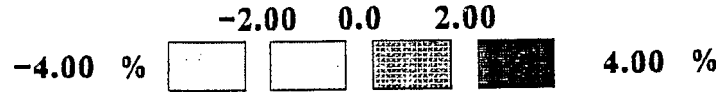

RESOLUTION

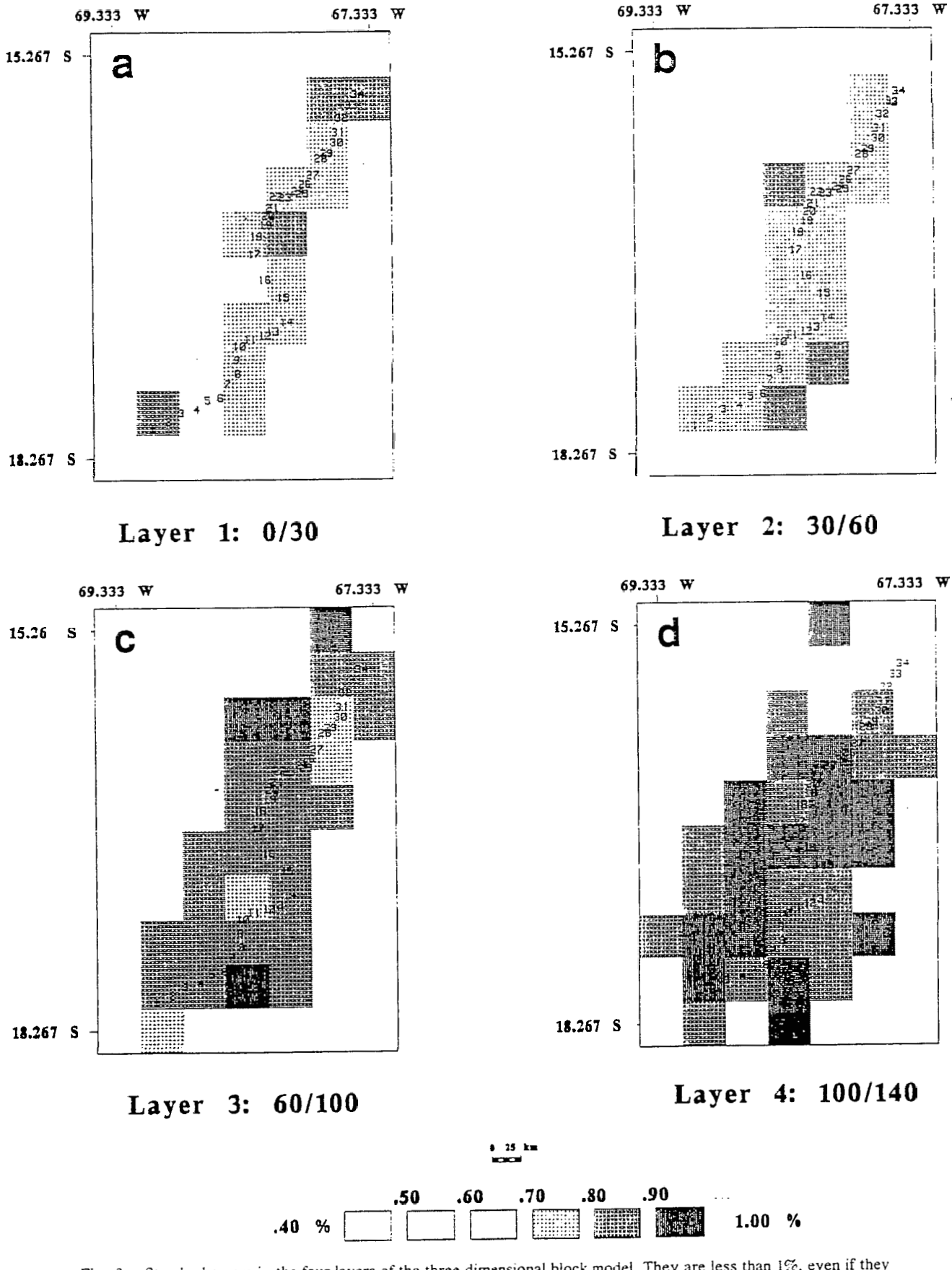

Fig. 8. Standard errors in the four layers of the three-dimensional block model. They are less than 1%, even if they increase in deeper layers.

of this three-dimensional inversion. Here we have chosen to present "synthetics" [*Spakman and Nolet*, 1988] which are much more easily read and are more meaningful than a resolution matrix. Synthetic residuals were computed using the actual ray geometry and a velocity model with the same layer thicknesses and blocks size as in the three-dimensional model to which alternating velocity perturbations of ±4% amplitude were added to the starting velocity of each block, resulting in the typical chess-pattern-like structure, commonly used in resolution tests [*Glahn et al.*, 1993]. In this way we obtained a structure where each block is surrounded by blocks of opposite sign in the velocity perturbation (see Figure 7). The model obtained by inversion of these synthetic residuals is presented in Figure 7 for the four layers. The central and southwestern part of the model shows sufficiently good resolution for all layers. In these zones, no change in the signs of the synthetic perturbations is observed, even in the deep layers. Figures 7*c* and 7*d* show clearly that the alternating velocity perturbations are also well recovered in the lower layers. However, the northeastern part shows very poor resolution for the second layer for blocks beneath the eastern flank of the Eastern Cordillera. This is clearly due to the lack of data in this region. Vertical coupling between neighboring layers has also been checked by analyzing the complete resolution matrix. Small values are obtained for the off-diagonal terms, indicating a low degree of coupling between adjacent blocks. Only a few marginal blocks show big values for the off-diagonal terms. An additional test, using only the *PKP* phases and *P* phases of events in the azimuth of the profile, has been performed giving the same pattern of velocity perturbations. Finally, we present in Figure 8 the standard errors for each resolved block. They vary from 0.4 to 0.9%, increasing with depth, and thus are acceptable. The standard errors of the largest perturbations are of the order of one magnitude smaller than the perturbations themselves.

In conclusion, the ray geometry used to compute the three-dimensional inversion model is able to resolve the structure with a good degree of accuracy beneath the profile down to a depth of 140 km; however, the second layer in the northeastern part is poorly constrained.

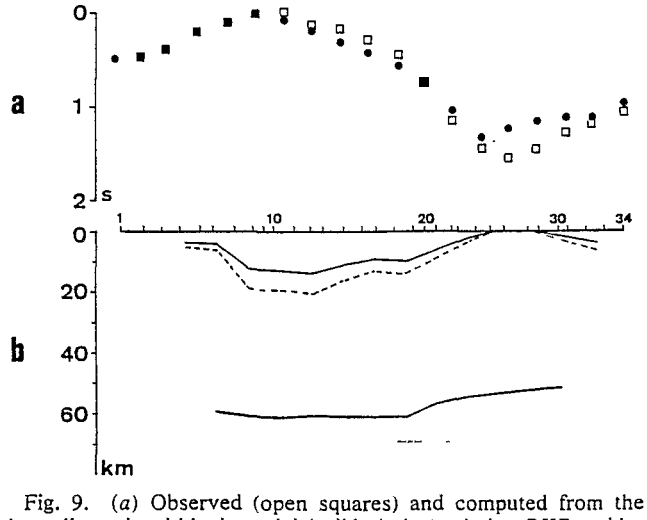

Fig. 9. (*a*) Observed (open squares) and computed from the three-dimensional block model (solid circles) relative *PKP* residuals, along the seismic profile. (*b*) Thickness of the sedimentary cover for two different realistic velocities (4.8 km/s (solid line) and 5.3 km/s (dashed line)) and depth of the Moho beneath the same profile.

TABLE 3. Relative Residuals Computed From the Inversion Result According to the Different Layers

	Zone 1/ Zone 2	Zone 3/ Zone 2	Zone 4/ Zone 2
Mean relative residual, s	−0.41	−0.30	−1.30
Layer 1			
ΔV, %	+8	+4	+12
R1, s	−0.41	−0.22	−0.60
Layer 2			
ΔV, %	0	+2	+7.5
R1, s		−0.09	−0.32
Crustal residual, s		−0.31	−0.92
Layers 3 and 4			
ΔV, %	0	0	+2.5
R1, s			−0.24
Total residual, s			−1.16

In order to remove the sharp changes in the velocity perturbations between adjacent blocks introduced by the "a priori" discretisation, the solution has been low-pass-filtered by using a bilinear interpolation function within each layer. Plates 2*a*–2*d* show the smoothed images of the three-dimensional block model presented on Figure 6. The first layer (Plate 2*a*) shows a well-marked low-velocity zone between stations 6 and 20, with a maximum velocity perturbation (more than −6%) beneath stations 8–12. A contrasting fast zone, with velocity perturbations greater than +4%, is observed to the east of station 25. A large velocity change (6%) is observed over a distance of less than 40 km, from −3% at station 18 to +3% at station 23. The velocity perturbations found are quite consistent with the conclusions based on the qualitative *P* delay time study and clearly agree with the geological structures previously described. Nearly the same pattern can be observed in the second layer which forms the lower part of the crust (Plate 2*b*); the low-velocity zone situated to the southeast of the profile, with a velocity contrast smaller than −2%, ends below the border of the Eastern Cordillera. The perturbations in the zone of high velocities, to the east of station 26, are higher than in the central zone of the Altiplano (+3% to +5%). Again the major change occurs beneath the Cordillera Real fault system.

This major boundary is also observed in the third layer, corresponding to the uppermost mantle (Plate 2*c*). However, the velocity contrasts are not as great as in the crust (−2% to +3%). While the slow-fast pattern is not as obvious below about 100 km depth, it is still present with the boundary between the contrasting zones being shifted slightly to the west.

A very simple test has been performed to check our final inversion model. We calculated the relative residuals for vertical *PKP* waves travelling throughout the three-dimensional block model beneath the stations. The values computed in this way have been plotted together with the interpolated mean *PKP* relative residuals observed along the profile (Figure 9*a*). The two curves agree well for the western and central part of the model; however, a shift of up to 0.3 s is observed in the eastern part of the profile, where the lowest observed values are situated. This discrepancy might correspond to the region where the lack of data is important and where we observe only a poor resolution in

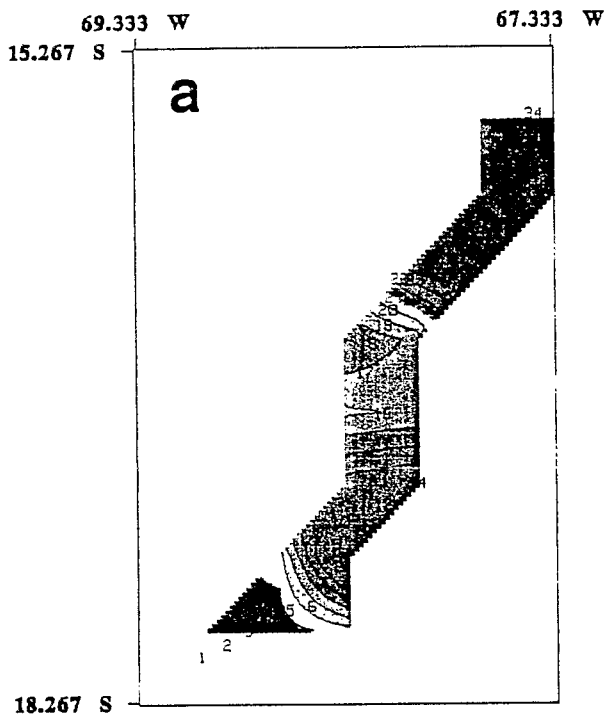

Layer 0-30

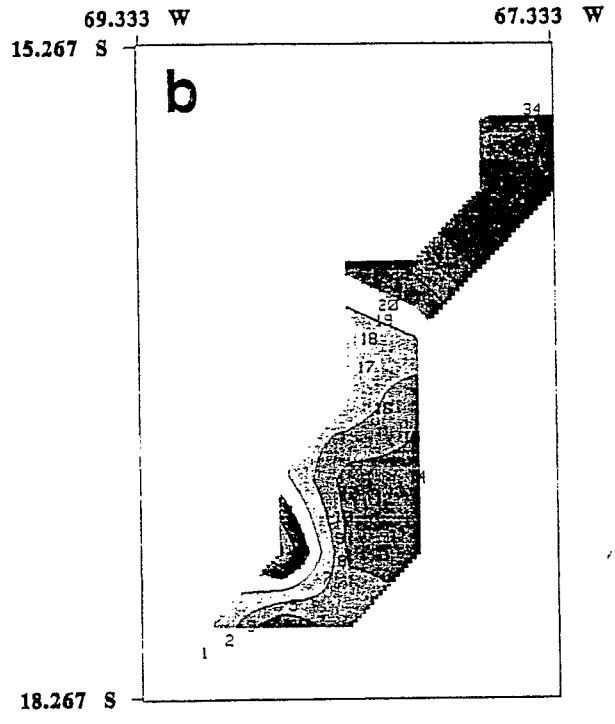

Layer 30-60

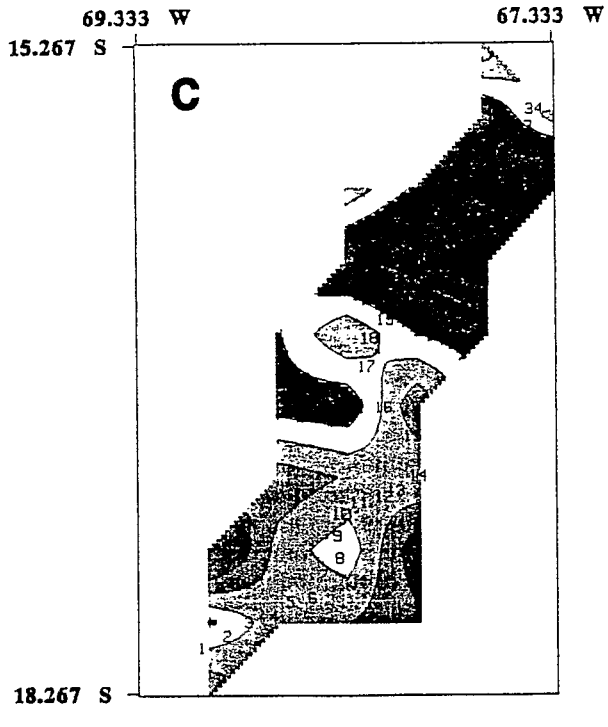

Layer 60-100

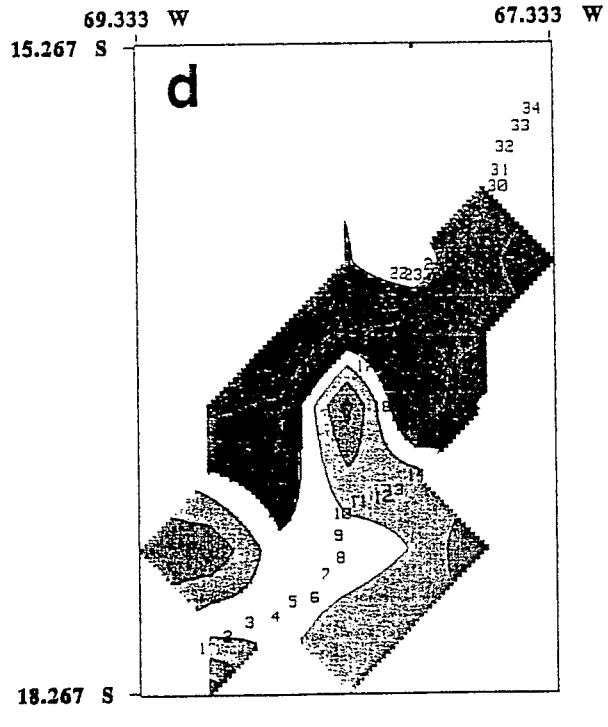

Layer 100-140

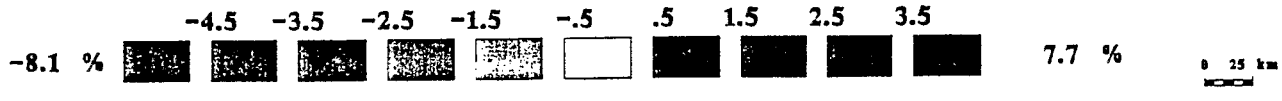

each layer (see Figure 7*b*). Thus the model resulting from the inversion, for which the contribution of vertical rays is a priori weak, explains reasonably well the shape and amplitude of *PKP* relative residuals, with the exception of the Eastern Cordillera.

In order to check which layer of the model contributes to the differences observed in relative *PKP* travel time residuals along the profile, stations 9, 10, and 11 (zone 2), in the Altiplano Basin, were taken as a reference, and we considered three homogeneous groups of stations: stations 3, 4, and 5 (zone 1), situated in the western Altiplano; stations 16, 17, and 18 (zone 3), on the western flank of the Eastern Cordillera; and stations 25–30 (zone 4), within the Eastern Cordillera. For these three zones (1, 3, and 4), we computed the residuals due to the velocity perturbation in each layer, relative to zone 2, and compared them to the observed relative residuals. The results, presented in Table 3, allow us to make a quantitative check and to improve the global pattern seen on the vertical cross section. The origin of the variations of the residuals is clearly different for the various zones. The relative residual of the first group (−0.41 s) is explained by the upper crust; in zone 3, velocity perturbations down to the Moho are needed to account for the relative residual (−0.30 s). In contrast, the value observed in zone 4 (−1.30 s) cannot be completely explained by the model. These results lead us to propose that structural differences between the Altiplano Basin and the western flank of the Cordillera on one side, and the Eastern Cordillera on the other side, are still present in the mantle below 140 km.

To conclude, the inversion results are consistent with the qualitative model, deduced from the *P* delay time analysis: that is, a slow central region and a fast region to the northeast. However, the main contribution of the inversion is to determine the depth of the contrast between these two zones. This contrast is essentially maintained throughout the depth range of the model, down to more than 120 km. The subvertical transition between the two zones is particularly well defined. The location of this boundary, which appears to be the major structural feature of the region under study, corresponds to the Cordillera Real fault system bounding the Eastern Cordillera on the west.

DISCUSSION AND INTERPRETATION

A vertical cross section through the three-dimensional model beneath the stations is shown in Plate 3*b*. This section has been extended down to 180 km in order to observe the deeper structures, although the resolution is very poor below 140 km. This kind of presentation is somewhat difficult to interpret, because the isovalue curves will incorrectly connect perturbations in the different layers. However, this simple picture emphasizes the quasi-vertical boundary between the low- and high-velocity zones. It also underlines the main difference between these two zones. Under the Altiplano, the large slow anomalies are confined to the crust, while the high-velocity zone under the Eastern Cordillera is quite marked down to 120 km. Moreover, it is worth noting the clear correspondence between the velocity perturbations and the geological cross section presented above (C. Martinez, manuscript in preparation, 1993) (Plate 3*a*). For example, the slow zone is present under the Altiplano, and its western border corresponds to the San Andres fault system. The zone of lowest velocities in the upper crust can clearly be correlated with the Altiplano Basin. The zone of high velocities is observed beneath the axial zone of the Eastern Cordillera and the sub-Andean zone; its western boundary corresponds to the fault system bordering the Cordillera to the west.

As the inversion was performed without any correction for the sedimentary cover, it is obvious that the velocity perturbations observed in the upper crustal layer are, at least partially, due to the sedimentary rocks. The Ordovician cover of the Eastern Cordillera, which is about 5 km thick, is deformed, metamorphosed, and intruded by Hercynian and Andean granites; thus its velocity is probably not very different from that of the basement, and when included in the computation, we find that it introduces a negligible effect in the residuals (less than 0.1 s). Considering that the faster zone in the first layer (Plate 2*a*), corresponding to the Eastern Cordillera, is free of sedimentary rocks from a velocity study point of view, we took it as a reference. We then assumed that the observed velocity differences relative to this zone are caused by the presence of thicker or thinner sedimentary infill. To keep the model simple and since the information on the *P* velocity values for the sedimentary rocks are scarce, we used only one specific velocity value as an approximation for the sedimentary cover, even though the age of the sedimentary rocks is not the same along the profile. The thicknesses obtained by doing so are shown on Figure 9*b* for two realistic velocities: 4.8 and 5.3 km/s [*Ocola and Meyer*, 1972; *Wigger*, 1988]. This gives the maximum sedimentary thickness (13 or 20 km, depending on the velocity used) between stations 8 and 13 in the Altiplano Basin. The sedimentary cover thins slightly on the western flank of the Cordillera (9 to 13 km from station 15 to 18) and decreases progressively under the mountain chain (from station 25 to 29). In the sub-Andean zone, east of station 30, it reaches about 4–6 km. All these calculated thicknesses for the sedimentary cover are quite realistic and are consistent with the geological data of the region. In the central Altiplano Basin, the values obtained for the thickness of sedimentary rocks are in agreement with the cumulated thickness proposed by *Meyer and Murillo* [1961] and *Ascarrunz* [1973*a*, *b*]. To the west of the profile, between stations 4 and 6, we find a sedimentary thickness of 3–5 km, consistent with the thickness of the Tertiary cover measured in a nearby borehole [*Lehman*, 1978]. Therefore, using a reasonable value for the velocity of the sedimentary rocks, all the perturbations in the first layer are explained by the sedimentary cover, and we do not need to introduce any lateral variation of the velocity in the basement. Nevertheless, if such variations exist, they are probably not very significant.

It is therefore reasonable to assume that the lower part of the crust (layer 2 in our model) is not strongly heteroge-

Plate 2. (Opposite) Smoothed velocity perturbations (in percent) in the four layers of the three-dimensional block model. To obtain the smooth pattern, we applied a bilinear interpolation function to the discrete perturbations within each horizontal layer. This smoothing algorithm preserves the amplitudes in individual central points of the original block discretization. Central coordinates of the model are 15.77°S, 68.33°W, and block sizes are 0.33° × 0.33°. Velocities higher than the reference correspond to positive values (blue end of the spectrum); velocities lower than the reference correspond to negative values (red end of the spectrum).

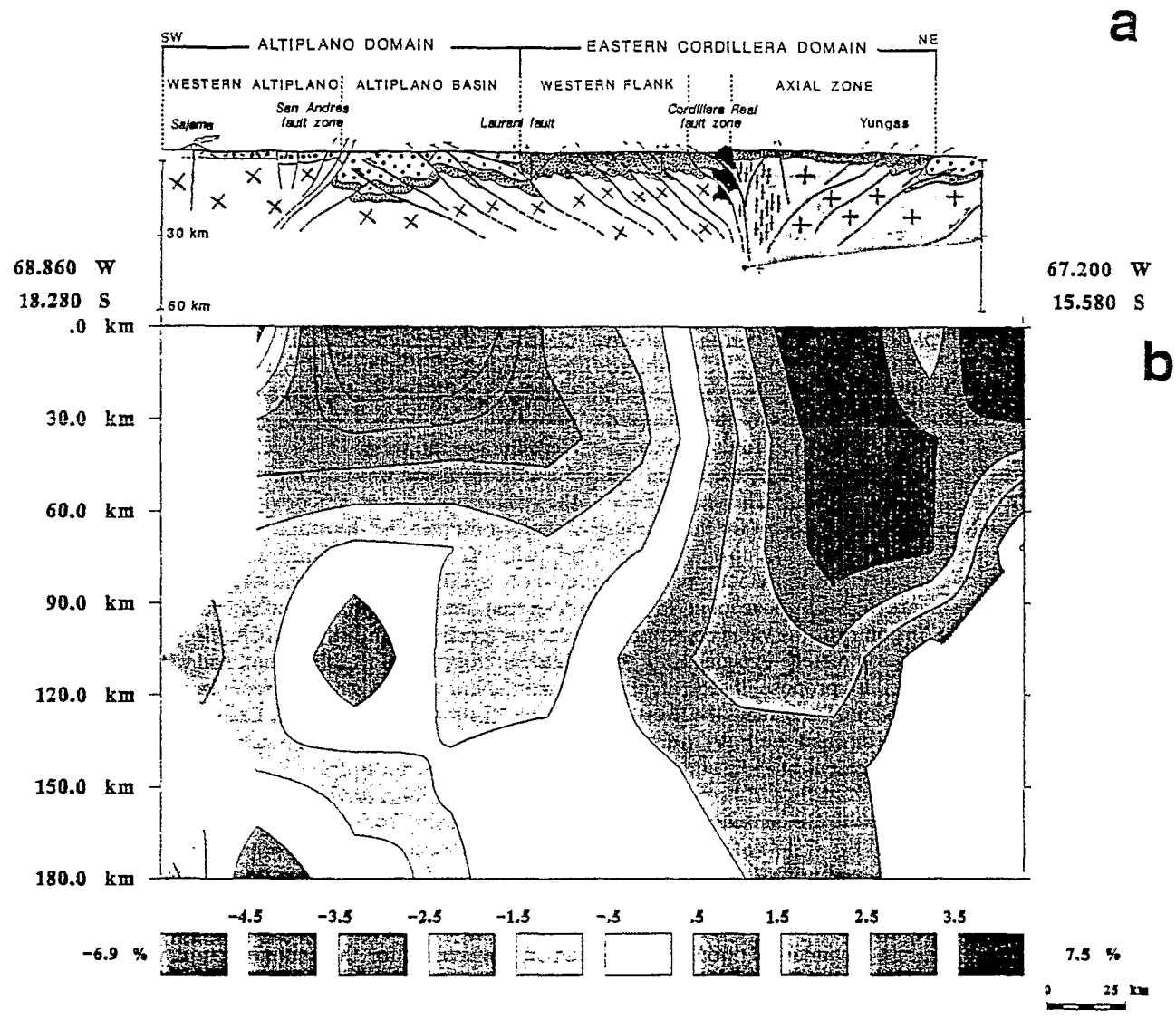

Plate 3. (*a*) Geological and structural cross section (from Figure 2*b*). (*b*) Vertical cross-section down to 180 km through the three-dimensional inversion model beneath the seismic profile, with the positions of the ends. The location of these profiles is shown on Figure 2*a*. Notice that the high-velocity zone (> +2.5%) is limited to the southwest, at least in the crust, by the Cordillera Real fault system.

neous. In this case, the velocity perturbations observed in the second layer can be explained by variations of the Moho depth. A simple computation leads to the results presented on Figure 8*b*. The crustal thickness is seen to be slightly more than 60 km beneath the Altiplano Basin and progressively thins to 50 km under the Eastern Cordillera.

Teleseismic inversion does not sufficiently constrain the absolute depth of the Moho. We have performed many trials covering the whole depth range provided by previous studies and the crustal thickness we finally selected for our initial model of 60 km, corresponds to a depth where velocity perturbations are clearly divided in organized zones. However, as the crustal basement is not strongly heterogeneous, the variation in the Moho depth is well constrained. Our study shows a nearly flat Moho from the west extending into the Cordillera Real fault system (stations 6–18), and the crust thins by 10 ± 1.5 km under the Eastern Cordillera. The thinning of the crust begins at the western border of the Eastern Cordillera, which again appears as an important feature. Unfortunately, the location of our profile does not allow us to sample the structure, either below the Western Cordillera or across the sub-Andes.

These results can be compared with previous studies based on different methods. In the model by *James* [1971], a crustal thickness of over 70 km beneath the Western Cordillera and the western part of the Altiplano is given, gradually diminishing to the east to 55–60 km below the Eastern Cordillera. Among the models deduced from gravity studies, the most recent one [*Fukao et al.*, 1989] shows a Moho depth of 65 km under the Western Cordillera and 55 km under the Eastern Cordillera with the crustal thickness changing smoothly between these two values below the Altiplano. Although these absolute values are also somewhat model-dependent, their relative amplitudes should be less so. These models which postulate the thinning of the crust by about 10 km from west to east are thus consistent with our results.

However, the form of this thinning is different because it is not progressive over the Altiplano but starts on its eastern border.

The elevation of the Eastern Cordillera is not very pronounced in relation to the plateau. Some very high peaks are present, but on the average, the chain itself is not a very prominent feature. Although an important root is not expected for such a narrow range, the thinning of the crust below the Cordillera clearly shows that it is not crustally, or at least not locally, compensated.

Let us compute the thickness of H of the crustal root necessary to compensate the average topography, $h = 3800$ m of the Altiplano. Taking $\rho = 2800$ kg/m^3 for the mean density of the crust and $\Delta\rho = -400$ kg/m^3 for the density difference between the crustal root and the mantle on either side [*Fukao et al.*, 1989], we find $H = 27$ km. Taking a crustal thickness of the order of 35–40 km under the Brazilian craton, we find a Moho depth of 62–67 km under the Altiplano. This value is quite compatible with the value deduced from our inversion model which is at 61 km depth. Thus our result, which is a little lower than the expected values, does not disagree with the hypothesis that the Altiplano is in isostatic equilibrium and, for the most part, crustally compensated.

Below 60 km, down to 140 km, velocities remain higher beneath the Eastern Cordillera where the perturbation reaches about 3%. This fast zone extends slightly to the west with increasing depth. The deep low-velocity zone beneath the Altiplano is not very obvious. In the western part of our model, a more prominent low-velocity zone is seen below 120 km, with perturbations as large as −3%.

A very likely hypothesis for this situation consists of associating the high-velocity zone to the east with a colder and/or older lithosphere than in the western part. In this case, the fast zone may represent the Brazilian craton. The underthrusting of the craton beneath the eastern margin of the Andes has been documented farther north in central Peru by *Suarez et al.* [1983] and *Dorbath et al.* [1991]. The underthrusting occurs along high-angle, deep active faults on the eastern side of the Andes. In southern Bolivia and northern Argentina, thin skin tectonics are more predominant as described by *Jordan et al.* [1983] and, more recently, by *Whitman et al.* [1992]. For a profile at 21°S they propose an underthrusted foreland beneath the sub-Andes with a maximum lithospheric thickness of 150 km beneath the Eastern Cordillera, and a thickened lid under the Altiplano, thinning to the west. In southern Bolivia, *Lyon-Caen et al.* [1985] propose underthrusting of the Brazilian shield under the Bolivian Andes to take into account the gravity anomalies. They estimate that the craton extends at least 150 km and possibly 200 km beneath the sub-Andes and the Eastern Cordillera, but they cannot really constrain the western limit of the underthrusting. Lastly, the study by *Roeder* [1988] implies as much as 230 km of underthrusting beneath the Eastern Cordillera along the line of the seismic traverse, taking place along a very low angle thrust. Our results are consistent with underthrusting of the Brazilian shield, associated with the high-velocity zone. Assuming this interpretation, our study places an important constraint on the present day western limit of the edge of the Brazilian craton beneath the Eastern Cordillera. Nevertheless our results are in contradiction with a low angle of underthrusting of this craton in the Central Andes.

The low-velocity zone may be associated to a hot mantle or a thinning of the lithosphere. The subduction of young oceanic lithosphere of the Nazca plate at a high speed (0.09 m/yr) for a substantial time (since the early Jurassic [*James et al.*, 1975]) could cause the build up of magmatic material from the western edge eastwards and thus produce hot mantle under the Altiplano. This is evidenced by the presence of active volcanoes in the Western Cordillera, where the subduction is normal, and a widespread volcanic activity coinciding with the highlands [*Froidevaux and Isacks*, 1984]. The isostatic equilibrium of the Altiplano is explained on the low side by a purely crustal root as noted before. The slow anomaly observed in the upper mantle beneath the Altiplano may be due to a slight thinning of the lithosphere. The unresolved combination of the crustal root and hot upper mantle proposed by *Froidevaux and Isacks* [1984] from their study of the geoid anomaly is not in contradiction with our results; since the slow velocity perturbations beneath the Altiplano are not very marked, we believe that the compensation is mainly crustal.

Our main result is the evidence of a subvertical contact, dipping slightly to the southwest, between two contrasting zones. This contact clearly corresponds at the surface to the Cordillera Real fault system. This study provides the first evidence for such a deep boundary in the Andes. Previous geophysical studies do not show this feature. This first teleseismic tomographic study presents new results, which can be explained by the location of our profile, in the change of trend of the Central Andes.

Based on our results, we propose the following hypothesis. First, the amplitude of the contrast in perturbations observed below 60 km could be due to a difference between cold and hot mantle. However, following *Estey and Douglas* [1986], to explain a velocity perturbation of 5%, a thermal contrast of 1000° is required, which is not very likely. Thus a mineralogical difference between the fast and slow zones could be present. As noted above, the Brazilian craton can be clearly associated with the deep high-velocity zone, but its underthrusting along a low-angle thrust cannot explain the observed subvertical deep contact. We therefore believe that the contact between two different lithospheric structures occurs along the Cordillera Real fault system. This fault system should mark the western boundary of the underthrusting of the Brazilian craton. In this case, the observed rise of the Moho beneath the western margin of the Eastern Cordillera could be explained effectively as a consequence of flexural support of the crust by the underthrust shield. The deep extension of this boundary also suggests that the system is very old and still active. In the western part, Precambrian rocks dated at 600 Ma have been found in the San Andres borehole [*Lehman*, 1978]. It seems realistic to assume that this suture is of the age as the Brazilide orogeny. Our seismic profile is located in the change of trend of the Central Andes, where the strike of the chain has never been perpendicular to the convergence direction, i.e., roughly east-west [*Larson and Pitman*, 1972; *Minster and Jordan*, 1978; *Withman et al.*, 1983]. We consider this suture as a transform fault. Field observations showing reverse faulting with a sinistral strike slip component are consistent with this hypothesis [*Martinez*, 1980; *Lavenu*, 1986]. Another consequence of this system could be the thick sedimentary filling in the subsiding Altiplano Basin which cannot be explained by the low angle underthrusting scenario. A

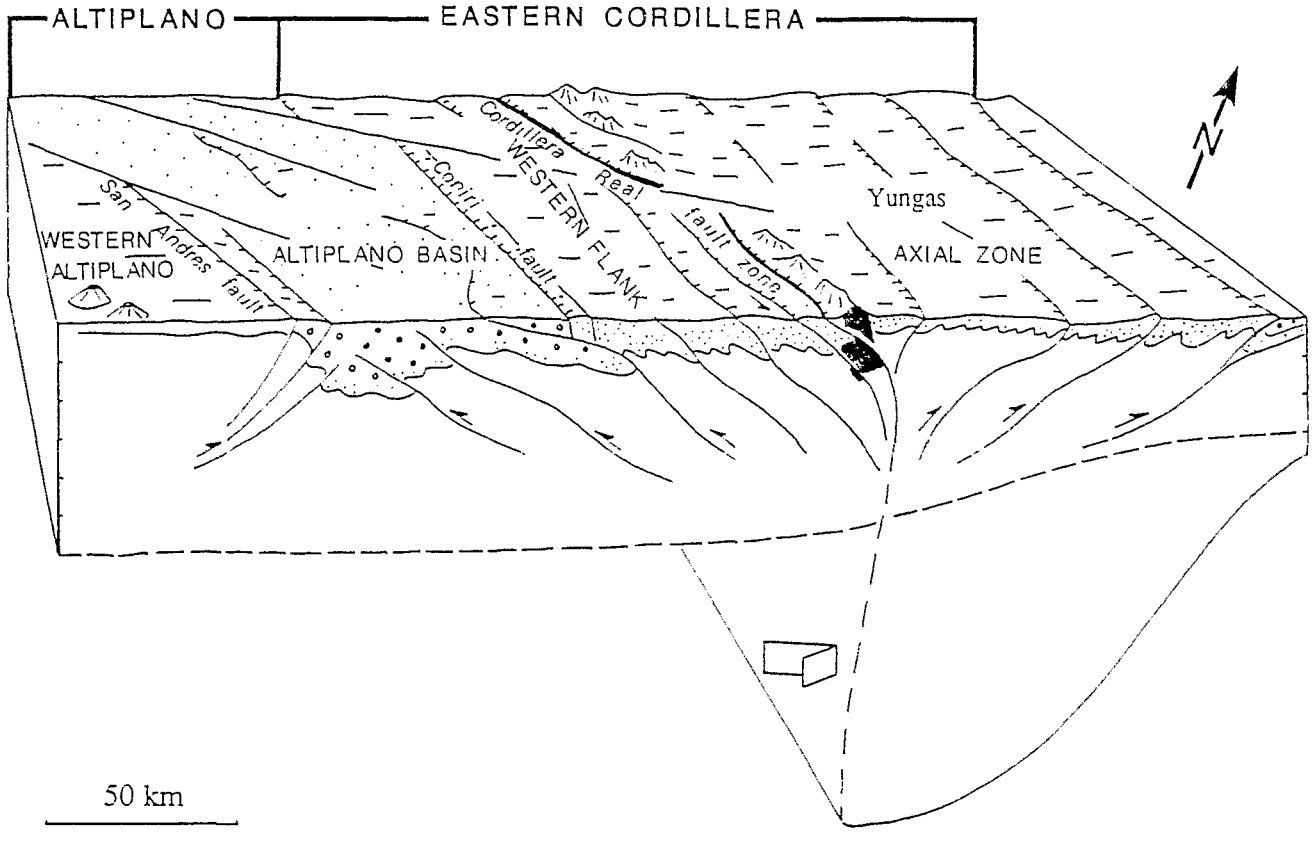

Fig. 10. Simplified sketch block diagram of the structures in northern Bolivia. The large arrow shows the relative movement (reverse faulting with a sinistral strike-slip component) between the two blocks. The extension in depth of the CRFZ symbolizes the old suture along which the decoupling between the two contrasted velocity blocks occurs.

schematic block diagram of our interpretative model is presented in Figure 10.

CONCLUSION

A teleseismic profile has been performed in northern Bolivia to map the velocity structure of the lithosphere-asthenosphere system beneath the Altiplano and the Eastern Cordillera. A careful study of relative travel time residuals led us to propose a simple qualitative model. The three-dimensional inversion mainly allowed us to specify the depth at which the lateral perturbations occur. The origin of the perturbations in the upper crust is reasonably accounted for by the variations in thickness of the sedimentary fill. The maximum of sedimentary rocks thickness, 12–20 km, is observed under the Altiplano Basin. The interpretation of the velocity perturbations in the lower crust as variations in Moho depth led us to propose a thinning of the crust from about 60 km under the Altiplano to 50 km under the Eastern Cordillera. The major feature of our model is a vertical boundary, dipping slightly to the southwest, which separates two strongly contrasting blocks throughout the model, from the surface down to 120 km. This boundary coincides at the surface with the Cordillera Real fault system, which is interpreted as an old suture zone. As the Altiplano is characterized by low velocities that are more pronounced in the crust, we interpret the high velocities beneath the Eastern Cordillera down to at least 120 km as the Brazilian craton. The subvertical nature of the contact between the craton and the western block leads us to infer that the underthrusting of the Brazilian shield does not occur along a low-angle thrust as was suggested in previous models. In the region of this study, corresponding to the change of trend of the Central Andes, the western limit of the underthrusting of the craton is clearly the western border of the Eastern Cordillera.

Acknowledgments. The authors would like to thank R. Cabré and all the team from the San Calixto Observatory in La Paz for their kind welcome and permanent help during this experiment; G. Herail, M. Launay, and the ORSTOM Centre in La Paz for the logistic assistance; G. Wittlinger, M. Lambert, L. Rivera, M. Bour, J. Trampert, I. Lecomte, J. J. Lévêque, and H. Haessler, who helped to install and maintain the mobile seismic network; Y. Liotier for providing his help for the imaging software; U. Achauer, W. J. Hinze, J. Helm, R. Truillet, and M. Seranne for improving the manuscript, M. Blanck for improving the figures. The manuscript benefited from critical reviews by D. Whitman and A. Snoke. We are indebted to the scientific council of the French Lithoscope Project for making us available the seismic stations. This project was sponsored by ORSTOM and INSU.

REFERENCES

Aki, K., A. Christoffersson, and E. S. Husebye, Determination of the three-dimensional seismic structure of the lithosphere, *J. Geophys. Res.*, *82*, 277–296, 1977.

Aki, K., 3-D inhomogeneities in the upper mantle, *Tectonophysics*, *75*, 31–40, 1981.

Ascarrunz, R., Estudio estructural de la region norte de la falla Coniri, *Bol. Soc. Geol. Boliv.*, *19*, 75–81, 1973*a*.

Ascarrunz, R., Contribucion al conocimiento geologico del area comprendida entre los pueblos de Viacha-Corocoro-y Umala, *Bol. Soc. Geol. Boliv.*, *20*, 29–64, 1973*b*.

Aubouin, J., A. V. Borrello, G. Cecioni, R. Charrier, P. Chotin, J. Frutos, R. Thiele, and J. C. Vicente, Esquisse paléogéographique et structurale des Andes méridionales, *Rev. Géogr. Phys. Géol. Dyn.*, *XV*(1–2), 11–72, 1973.

Audebaud, E., R. Capdevila, B. Dalmayrac, J. Debelmas, G. Laubacher, C. Lefevre, R. Marocco, C. Martinez, M. Mattauer, J. P. Paredes, and P. Tomasi, Les traits géologiques essentiels des Andes Centrales (Pérou-Bolivie), *Rev. Géogr. Phys. Géol. Dyn.*, *XV*(1–2), 73–114, 1973.

Babuska, V., J. Plomerova, and J. Sileny, Large-scale oriented structures in the subcrustal lithosphere of central Europe, *Ann. Geophys.*, *2*, 649–662, 1984.

Baby, P., T. Sempere, J. Oller, L. Barrios, G. Herail, and R. Marocco, Un bassin en compression d'age oligo-miocène dans le sud de l'Altiplano Bolivien, *C. R. Acad. Sci.*, *311*, 341–347, 1990.

Bard, J. P., R. Botello, C. Martinez, and T. Subieta, Relations entre tectonique, métamorphisme et mise en place d'un granite éohercynien à deux micas dans la Cordillère Real de Bolivie (Massif de Zongo-Yani), *Cah. ORSTOM. Sér. Géol.*, *6*(1), 3–18, 1974.

Bourgois, J., and D. Janjou, Subduction océanique, subduction continentale et subduction andine, *C. R. Acad. Sci.*, *292*, 859–864, 1981.

Cabré, R., Geophysical studies in central Andes, in *Geodynamics of the Eastern Pacific Region, Caribbean and Scotia Arcs, Geodyn. Ser.*, vol. 9, edited by R. Cabré, pp. 73–77, 1983.

Cisternas, A., Crustal structure of the Andes from Rayleigh wave dispersion, *Bull. Seismol. Soc. Am.*, *51*, 381–388, 1961.

Cobbing, E. J., J. M. Ozard, and N. J. Snelling, Reconnaissance geochronology of the cristalline basement rocks of the coastal Cordillera of southern Peru, *Geol. Soc. Am. Bull.*, *88*, 241–246, 1977.

Dalmayrac, B., G. Laubacher, and R. Marocco, Caractères généraux de l'évolution géologique des Andes péruviennes, *Trav. Doc. ORSTOM*, *122*, 507 pp., 1980.

Dewey, J. F., and J. M. Bird, Mountain belts and the new global tectonics, *J. Geophys. Res.*, *75*, 2625–2647, 1970.

Dorbath, L., C. Dorbath, E. Jimenez, and L. Rivera, Seismicity and tectonic deformation in the Eastern Cordillera and the sub-Andean zone of central Peru, *J. South Am. Earth Sci.*, *4*, 13–24, 1991.

Dziewonski, A. M., and D. L. Anderson, Travel times and station corrections for *P* waves at teleseismic distances, *J. Geophys. Res.*, *88*, 3295–3314, 1983.

Estey, L. H., and B. J. Douglas, Upper mantle anisotropy: A preliminary model, *J. Geophys. Res.*, *91*, 11,393–11,406, 1986.

Evans, J. R., and U. Achauer, Teleseismic velocity tomography using the ACH method: Theory and application to continental-scale studies, in *Seismic Tomography: Theory and Practice*, edited by H. M. Iyer and K. Hirahara, Chapman and Hall, London, in press, 1993.

Fernandez, L. M., and J. Careaga, The thickness of the crust in central United States and La Paz, Bolivia, from the spectrum of longitudinal seismic waves, *Bull. Seismol. Soc. Am.*, *58*, 711–741, 1968.

Froidevaux, C., and B. L. Isacks, The mechanical state of the lithosphere in the Altiplano-Puna segment of the Andes, *Earth Planet. Sci. Lett.*, *71*, 305–314, 1984.

Fukao, Y., A. Yamamoto, and M. Kono, Gravity anomaly across the Peruvian Andes, *J. Geophys. Res.*, *94*, 3867–3890, 1989.

Glahn, A., M. Granet, U. Achauer, and the Rhine Graben Teleseismic Group (Y. Liotier, P. D. Slack, and G. Wittlinger), Southern Rhine Graben: Small-wavelength tomographic study and its implication on the graben's dynamic evolution, *Geophys. J. Int.*, in press, 1993.

Herrin, E., Seismological tables for *P* phases, *Bull. Seismol. Soc. Am.*, *58*, 1193–1242, 1968.

Isacks, B. L., Uplift of the Central Andean Plateau and Bending of the Bolivian Orocline, *J. Geophys. Res.*, *93*, 3211–3231, 1988.

James, D. E., Andean crustal and upper crustal mantle structure, *J. Geophys. Res.*, *76*, 3246–3271, 1971.

James, D. E., C. Brooks, and A. Cuyubamba, Early evolution of the central Andes volcanic arc, *Year Book Carnegie Inst. Washington*, *74*, 274–324, 1975.

Jeffreys, H., and K. E. Bullen, *Seismological Tables*, 50 pp., Office of the British Association, London, 1970.

Jordan, T. E., B. L. Isacks, R. W. Allmendinger, J. A. Brewer, V. A. Ramos, and C. J. Ando, Andean tectonics related to geometry of subducted Nazca plate, *Geol. Soc. Am. Bull.*, *94*, 341–361, 1983.

Kono, M., Y. Fukao, and A. Yamamoto, Mountain building in the Central Andes, *J. Geophys. Res.*, *94*, 3891–3905, 1989.

Larson, R. L., and W. C. Pitman III, World-wide correlation of Mesezoic magnetic anomalies, and its implications, *Geol. Soc. Am. Bull.*, *83*, 3645–3662, 1972.

Lavenu, A., Etude néotectonique de l'Altiplano et de la Cordillère Orientale des Andes Boliviennes, thèse doc. etat, 433 pp., Univ. de Orsay, France, 1986.

Lehmann, B., A Precambrian core sample from the Altiplano/Bolivia, *Geol. Rundsch.*, *67*, 270–278, 1978.

Lyon-Caen, H., P. Molnar, and G. Suarez, Gravity anomalies and flexure of the Brazilian shield beneath the Bolivian Andes, *Earth. Planet. Sci. Lett.*, *75*, 81–92, 1985.

Martinez, C., Structure et évolution de la chaîne Hercynienne et de la chaîne Andine dans le nord de la cordillère des Andes de Bolivie, *Trav. Doc. ORSTOM*, *119*, 351 pp., 1980.

Martinez, C., and M. Seguret, Les bassins tertiaires de l'Altiplano sont-ils des bassins flexuraux intrachaine?, Col. Int. "Géodyn. Andine", Off. de la Rech. Sci. et Tech. Outre-Mer, Paris, 1990.

Martinez, C., and P. Tomasi, Carte structurale des Andes septentrionales de Bolivie, *Not. Explicative 77*, 48 pp., Off. de la Rech. Sci. et Tech. Outre-Mer, Paris, 1978.

Martinez, C., P. Tomasi, B. Dalmayrac, G. Laubacher, and R. Marocco, Caractères généraux des orogènes Précambrien, Hercynien et Andin au Pérou et en Bolivie, paper presented at 24th International Congress, section 1, Int. Union of Geod., Montréal, Que., 1972.

McBride, S., R. C. R. Robertson, A. H. Clark, and E. Farrar, Magmatic and metallogenic episodes in the northern tin belt, Cordillera Real, Bolivia, *Geol. Rundsch.*, *72*, 685–714, 1983.

Megard, F., B. Dalmayrac, G. Laubacher, R. Marocco, C. Martinez, J. Paredes, and P. Tomasi, La chaine hercynienne au Pérou et en Bolivie, Premiers résultats, *Cah. ORSTOM. Sér. Géol.*, *3*(1), 5–44, 1971.

Meyer, H. C., and F. J. E. Murillo, Sobre la geologia en las provincias Aroma, Pacajes y Carangas, *Bol. Dep. Nac. Geol.*, *1*, 149 pp., 1961.

Minster, J. B., and T. H. Jordan, Present-day plate motions, *J. Geophys. Res.*, *83*, 5331–5354, 1978.

Ocola, L. C., and R. P. Meyer, Crustal low-velocity zones under the Peru-Bolivia Altiplano, *Geophys. J. R. Astron. Soc.*, *30*, 199–209, 1972.

Ocola, L. C., R. P. Meyer, and L. T. Aldrich, Gross crustal structure under Peru-Bolivia Altiplano, *Earthquakes Notes*, *42*, 3–4, 33–48, 1971.

Roeder, D., Andean-age structure of Eastern Cordillera (Province of La Paz, Bolivia), *Tectonics*, *7*, 23–39, 1988.

Rutland, R. W. R., Andean orogeny and sea floor spreading, *Nature*, *233*, 252–255, 1971.

Schmucker, U., S. Forbush, O. Hartmann, A. Giesecke, M. Casaverde, J. Castillo, R. Salgueiro, and S. Del Pozo, Electrical conductivity anomaly under the Andes, *Year Book Carnegie Inst. Washington*, *65*, 11–28, 1966.

Sempere, T., G. Herail, J. Oller, and M. G. Bonhomme, Late Oligocene–early Miocene major tectonic crisis and related basins in Bolivia, *Geology*, *18*, 946–949, 1990.

Sheffels, B. M., Structural constraint on crustal shortening in the Bolivian Andes, Ph.D. thesis, 170 pp., Mass. Inst. of Technol., Cambridge, 1988.

Sheffels, B. M., Lower bound on the amount of crustal shortening in the central Bolivian Andes, *Geology*, *18*, 812–815, 1990.

Spakman, W., and G. Nolet, Imaging algorithms, accuracy and resolution in delay time tomography, in *Mathematical Geophysics*, edited by N. J. Vlaar, G. Nolet, M. J. R. Wortel, and S. A. P. L. Cloetingh, pp. 155–187, D. Reidel, Norwell, Mass., 1988.

Strunk, S., Analyse und Interpretation des Schwerefeldes des aktiven Kontinenralrandes des zentralen Anden (20°–26°S), Berl. Geowiss. Abh., *Reihe B*, *17*, 135 pp., 1990.

Suarez, G., P. Molnar, and B. C. Burchfiel, Seismicity, fault plane

solutions, depth of faulting, and active tectonics of the Andes of Peru, Ecuador, and southern Colombia, *J. Geophys. Res.*, *88*, 10,403–10,428, 1983.

Tatel, H. E., and M. A. Tuve, Seismic studies in the Andes, *Eos Trans. AGU*, *39*, 580–582, 1958.

Uyeda, S., and H. Kanamori, Back-arc opening and the mode of subduction, *J. Geophys. Res.*, *84*, 1049–1061, 1979.

Whitman, D., L. Isacks, J. L. Chatelain, J. M. Chiu, and A. Perez, Attenuation of high-frequency seismic waves beneath the Central Andean Plateau, *J. Geophys. Res.*, *97*, 19,929–19,947, 1992.

Whitman, J. M., C. G. Harrison, and G. W. Brass, Tectonic evolution of the Pacific Ocean since 74 Ma, *Tectonophysics*, *99*, 241–249, 1983.

Wigger, P., Seismicity and crustal structure of the central Andes, in *The Southern Central Andes. Lect. Notes Earth Sci.*, vol. 17, edited by H. Bahlburg, C. Breitkreuz, and P. Giese, pp. 209–229, Springer-Verlag, New York, 1988.

C. Dorbath and M. Granet, EOPGS, 5 rue Rene Descartes, 67084 Strasbourg Cedex, France.

C. Martinez, Laboratoire de Géologie des Bassins, 34095 Montpellier Cedex 5, France.

G. Poupinet, LGIT IRIGM, BP 53X, 38041 Grenoble Cedex, France.

(Received December 23, 1991;
revised September 28, 1992;
accepted October 6, 1992.)